EFFECTIVE INTERACTIONS BETWEEN LOCAL HOPPING MODULATIONS ON THE SQUARE LATTICE

A Dissertation
presented in partial fulfillment of requirements
for the degree of Master of Science
in the Department of Physics and Astronomy
The University of Mississippi

by

Huu T Do

December 2017

ABSTRACT

I have constructed the Ruderman-Kittel-Kasuya-Yosida (RKKY) interaction between Ising spin variables living on the link of the square lattice. The interaction is mediated by itinerant fermions, which couple to the Ising spin in the form of a hopping modulation. I consider the system at the half-filling and for two different values of the external magnetic field: $\mathbf{B} = \mathbf{0}$ produces Fermi surface (Fermi band), and $\mathbf{B} \neq \mathbf{0}$ gives Fermi points (Dirac band). The RKKY interaction between Ising spins in the "link model", is compared to the result for spins at each vertex or "site model" to determine the macroscopic magnetic order. For the zero-flux square lattice ($\mathbf{B} = \mathbf{0}$), the strong nesting property of the Fermi surface determines the magnetic ordering vectors. In shifting the spin from site to link, the magnetic interaction formally acquires a 2×2 matrix structure. The magnetic order of the "site model" is found to conventional antiferromagnetic (type-G AFM) and stripe AFM for "link model". For the π-flux square lattice ($\mathbf{B} \neq \mathbf{0}$), the RKKY interactions show 2×2 and 4×4 matrix structures for the "site model" and "link model", respectively. Their magnetic ordering vectors differ on their cases because of the collapsing of the Fermi surface to Fermi points. The system develops type-A AFM and ferrimagnetic order in the site and link models, respectively.

DEDICATION

I, HUU T. DO, declare that this thesis titled, "Effective interactions between local hopping modulations on the π-flux square lattice" and the work presented in it are my own. I confirm that:

- This work was done wholly or mainly while in candidate for a research degree at this University.
- Where any part of this thesis has previously been submitted for a degree or any other qualification at this University or any other institution, this has been clearly stated.
- Where I have consulted the published work of others, this is always clearly attributed.
- Where I have quoted from the work of others, the source is always given. With the exception of such quotations, this thesis is entirely my own work.
- I have acknowledged all main sources of help.
- Where the thesis is based on work done by myself jointly with others, I have made clear exactly what was done by others and what I have contributed myself.

ACKNOWLEDGEMENTS

I take this opportunity to say thanks to my advisor, department, committee members, colleagues, and family.

First and foremost, I strongly appreciate my advisor, Dr. Beach who has guided me in research on this interesting topic. My undergraduate background is in experimental physics, so my theoretical knowledge is initial weak. Switching my field has been fascinating work, but it is a really challenging jump. My project uses quantum mechanics, applied to condensed matter physics, to derive the magnetic interaction. Therefore, I have failed a thousand times to get the correct result. Luckily, Dr. Beach is patient and dedicated to help me pass these obstacles. He also shows with me interesting information about the strongly correlated electrons in condensed master physics. It is so helpful for me to develop my background of magnetism and superconductivity, which I want to pursue in my future career.

Second, I would like to thank our Department of Physics and Astronomy at the University of Mississippi for supporting me to do research during summer time. I also say thank to Vietnam Education Foundation (VEF), which provide a scholarship to help me study in the United States. I also want to say many thanks to the Mississippi Center for Supercomputing Research, which has hosted my running code.

Let me say thanks to my committee members, Dr. Bombelli and Dr. Zhang. They spent time to look at my thesis and give useful comments. I also appreciate my labmate, Khagendra Adhikari for helping me with the C++ code.

Last but not least, I would like to appreciate my family, my daughter and wife. Without them, I would not have stayed motivated to complete my work.

TABLE OF CONTENTS

LIST OF FIGURES

CHAPTER 1

INTRODUCTION

1.1 Tight binding electrons

1.1.1 Sommerfeld and Bloch wave functions

In this section, I will introduce different models of free electrons (free in the sense of no interaction potential) in solid materials including the Sommerfeld (free electron, or plane wave approximation), Bloch (nearly free electron with constant periodic potential), and Wannier (tight binding model) wave functions. When electrons are unbound in solid materials, the important parameters are the wave function and energy dispersion relation (single-particle energy function in momentum space) to define their properties. Let us start with the general Schrödinger equation in real space [5]:

$$\hat{H}\psi(\mathbf{R}) = E\psi(\mathbf{R}). \tag{1.1}$$

Here, $\hat{H}$ is the total Hamiltonian of the system, E is the eigenenergy, and $\psi(R)$ is the eigenfunction of an electron in real space $\mathbf{R}$.

Sommerfeld model — In the Sommerfeld model, the electron is free to propagate inside the material with kinetic Hamiltonian $\hat{H} = \frac{\mathbf{p}^2}{2m}$, so the Schrödinger equation is

$$-\frac{\hbar^2}{2m}\left(\frac{\partial^2}{\partial x^2} + \frac{\partial^2}{\partial y^2} + \frac{\partial^2}{\partial z^2}\right)\Psi(\mathbf{r}) = E\Psi(\mathbf{r}). \tag{1.2}$$

Assuming periodic boundary conditions, the eigenenergy and eigenfuction are

$$E(\mathbf{k}) = \frac{\hbar^2 \mathbf{k}^2}{2m}, \tag{1.3}$$

$$\Psi_{\mathbf{k}}(\mathbf{r}) = \frac{1}{\sqrt{V}} e^{i\mathbf{k}\cdot\mathbf{r}}. \tag{1.4}$$

where $\mathbf{k}$ is the momentum vector, and V is the volume of the box. Level surfaces of the energy dispersion in momentum space form spherical shells for the three dimensional (3D) case and circles for the two dimensional (2D) case. The wave function $\Psi_{\mathbf{k}}(\mathbf{r})$ is the plane wave. The Sommerfeld model is applied to explain the electrical and thermal properties of some alkali metals such as Na, K, and Cs [5].

Bloch model — In the Bloch model (or nearly free electron model), the Hamiltonian includes a weak periodic potential $U(\mathbf{r}+\mathbf{R}) = U(\mathbf{r})$ (with some fixed translation vectors $\mathbf{R}$), representing the ionic background:

$$\hat{H}\Psi(\mathbf{r}) = \left[-\frac{\hbar^2}{2m}\bigtriangledown^2 + U(\mathbf{r}) \right] \Psi(\mathbf{r}) = E\Psi(\mathbf{r}). \tag{1.5}$$

The energy dispersion of a Bloch electron is labeled by a band index n. There is no explicit form of the energy dispersion relation $E_n(\mathbf{k})$. It is periodic in the reciprocal lattice: $E_n(\mathbf{k}+\mathbf{K}) = E_n(\mathbf{k})$, where $\mathbf{K}$ is the reciprocal vector. The wave function is written in terms of the band index n and wave vector $\mathbf{k}$: $\Psi_{n\mathbf{k}} = e^{i\mathbf{k}\cdot\mathbf{r}} u_{n\mathbf{k}}(\mathbf{r})$, where the function $u_{n\mathbf{k}}(\mathbf{r})$ has the periodicity of the potential.

Bloch model can explain very well the properties of many solid materials that are categorized as simple band of metals, semiconductors, semimetals, and insulators. Let us consider serveral concepts arisen from this treatment.

First, the Brillouin zone is defined as the set of nonequivalent points in momentum space. The first Brillouin zone contains all energy levels whose occupation defines the electronic properties.

The Fermi surface E_F is a constant energy surface (or a set of constant energy surfaces) in k-space (or momentum space), familiar to equipotentials of electrostatic theory with constant energy. The Fermi surface separates occupied and unoccupied electronic levels.

The band gap is an important quantity that determines the properties of the solid materials. It is the difference in energy between the highest occupied level and the lowest unoccupied level. The band gap and Fermi level are useful parameters to classify conventional materials into metal, semimetal, semiconductor, and insulator. For example, metals have no band gap and Fermi level always pass through an energy band. Semiconductors have a small energy gap (e.g Si has a band gap of 1.1 eV), and the Fermi level lives inside the band gap. Semimetals have no band gap, but the Fermi surface lives at the point contacting between two energy bands [5].

1.1.2 Tight-binding electron model

Bloch wave function understood to describe a gas of nearly free electrons, weakly perturbed by the constant periodic potential of the ions. The tight-binding or linear combination of atomic orbitals (LCAO) approach regards the materials as a collection of weakly interacting neutral atoms. The tight-binding approximation make use of the overlap of atomic wave functions between isolated atoms. This approximation is useful to describe the energy band of partially filled d-shell, f-shell atoms (Co, Fe, Ni, Gd, and other magnetic elements), and the electronic structure of insulators.

One assumes that in the vicinity of each lattice point, the full periodic crystal Hamiltonian $\hat{H}$ can be approximated by the atomic Hamiltonian, $\hat{H}_{\mathrm{at}}$, of a single atom at the lattice point. This is reasonable if the bound levels of the atomic Hamiltonian

are well-localized. Then,

$$\hat{H}\Psi_n = E_n\Psi_n, \tag{1.6}$$

$$\hat{H} = \hat{H}_{\rm at} + \Delta U(\mathbf{r}), \tag{1.7}$$

where $\Delta U(\mathbf{r})$ includes all corrections to the atomic potential required to produce the full periodic potential of the crystal. The Bloch wave function can also be constructed from N linear combinations of the degenerate tight-binding orbital wave function,

$$\Psi(\mathbf{r}+\mathbf{R}) = e^{i\mathbf{k}\cdot\mathbf{R}}\Psi(\mathbf{r}), \tag{1.8}$$

$$\Psi_{n\mathbf{k}}(\mathbf{r}) = \sum_{\mathbf{R}} e^{i\mathbf{k}\cdot\mathbf{R}}\Psi_n(\mathbf{r}-\mathbf{R}). \tag{1.9}$$

Here, n is the band index, and the momentum $\mathbf{k}$ ranges through the N points in the first Brillouin zone. The real space wave function $\Psi(\mathbf{r})$ is written in terms of basic functions $\phi_n(\mathbf{r})$ and creation $c^\dagger_{j\sigma}$ and annihilation $c_{j\sigma}$ operators (with σ denoting z-axis projection of the z-direction Pauli spin matrix):

$$\hat{\Psi}_\sigma(\mathbf{r}) = \sum_j \phi_j(\mathbf{r})c_{j\sigma}(\mathbf{r}), \tag{1.10}$$

$$\hat{\Psi}^*_\sigma(\mathbf{r}) = \sum_j \phi^*_j(\mathbf{r})c^\dagger_{j\sigma}(\mathbf{r}). \tag{1.11}$$

The hopping integral t_{ij} (i and j are nearest-neighbor atoms) is calculated from the kinetic term of the Hamiltonian:

$$\begin{aligned} t_{ij} &= \int d^3\mathbf{r}\phi^*(\mathbf{r}-\mathbf{r}_i)\hat{H}_{at}\phi(\mathbf{r}-\mathbf{r}_j) \\ &\approx \int d^3\mathbf{r}\phi^*(\mathbf{r}-\mathbf{r}_i)\bigg(-\frac{\hbar^2}{2m}\bigtriangledown^2\bigg)\phi(\mathbf{r}-\mathbf{r}_j). \end{aligned} \tag{1.12}$$

Each contribution to the Hamiltonian $\hat{H}_{\rm at}$ is a product of energy dispersion relation

$\varepsilon_{\mathbf{k}\sigma}$ (a function of momentum) and the number operator $\hat{N}_{\mathbf{k}\sigma} = c^{\dagger}_{\mathbf{k}\sigma} c_{\mathbf{k}\sigma}$.

$$\hat{H}_{\mathrm{at}} = \sum_{\mathbf{k}\sigma} \varepsilon_{\mathbf{k}\sigma} \hat{N}_{\mathbf{k}\sigma}. \tag{1.13}$$

In this work, we have applied the tight-binding model under the assumption of a constant hopping integral ($t_{ij} = \mathrm{const}$) between the nearest-neighbor sites on the square lattice.

1.2 π-flux model

Affleck *et al.* originally proposed the π-flux model of fermions on the square lattice in order to explain the properties of CuO_2 planes in high-T_c superconductors [2]. With application of a constant magnetic field, the magnetic flux changes the hopping integral t_{ij} from real values to a complex ones, according to the Aharonov-Bohm effect [30]. Now, the hopping integral of the nearest-neighbor bond $\langle ij \rangle$ is given by $t_{ij} = -te^{i\phi_{ij}}$ (with t: a real constant), and $\phi_{ij} = -\phi_{ji} = (e/\hbar c) \int_i^j \mathbf{A} \cdot d\mathbf{l}$, $\mathbf{A}$ is the vector potential, treated as classical variable [17]. Because of gauge invariance, the phase of t_{ij} can be adjusted with two real values when $\phi_{ij} = 0$ or π. Without π-flux, tight-binding model of the square lattice gives the definite Fermi surface at the half-filling. However, by inserting the π-flux, the Fermi surface shrinks into four Dirac points around which the energy dispersion relation is linear forming a Dirac cone. This is similar to the Dirac cones appearing in the hexagonal lattice of graphene.

The π-flux model have recently reemerged in the context of coupling it to a Transverse Field Ising spin such models having Dirac fermions sitting at the vertices of square lattice, and Ising spin variable at the links. They show the rich variety of ground state phases [16, 36]. First, X. Y. Xu *et al.* showed the second-order Ising quantum spin and first-order topological phase transition belong to weak and intermediate coupling between Dirac fermions and Ising spin [36]. Second, S. Gazit and his colleagues found

that at generic filling (change the chemical potential in partition function), the gauge fluctuations mediate pairing which leads to a transition between deconfined BCS state (Bardeen-Cooper-Schrieffer model explained the mechanism of metallic superconductor at low temperature) and confined BEC state (Bose-Einstein condensation) [16].

1.3 RKKY interaction

1.3.1 Kondo lattice model

The Kondo model was proposed to explain the measurement of anomalous resistance by doping dilute magnetic impurities in non-magnetic hosts. The resistance versus temperature (ρ–T) of pure non-magnetic metals, such as Na, K, Ag, and Cu, is decreased to a residual value when temperature goes down to zero. However, when non-magnetic elements (Cu, Ag, and Al) are doped with magnetic elements such as Fe, Mn, and Co. They observed the minimum resistivity at a finite temperature T that was from 10 to 20 K [20, 21]. In the 1970s, Kondo explained theoretically that mechanism based on the interaction between localized spin of magnetic impurities and the spin of itinerant electrons [21]. The minimum value of T is called Kondo temperature T_{K}. Therefore, the Kondo lattice model includes itinerant electrons and localized spin degrees of freedom which are coupled together.

In various systems, a lattice of localized spins and itinerant electrons coexists. Examples include rare-earth elements (Gd, Dy), rare-earth alloys ($CeCu_2Si_2$, $CeAl_3$, $CeAl_2$) and actinide compounds (U_2Zn_{17}, UCd_{11}, U_2PdSi_3) [8]. Depending on the coupling J between the localized spins with free electrons, many ground states develop. In figure 16.16 of reference [11], Piers Coleman shows for weak interaction if $J < 0$, the ferromagnetic order (FM) happens, if $J > 0$ the anti-ferromagnetic (AFM) state emerges. For the strong coupling, the Kondo singlet pair between localized spin and free electron formed to paramagnetic state or Fermi liquid. Because of that coupling,

the some materials can tranform from metal to insulator (Mott insulator) by changing chemical composition, pressure or magnetic field. Furthermore, S. Doniach showed that in Kondo lattice model, there is a competing energy scale between Kondo singlet (Kondo effect) and RKKY interaction [13]. The characteristic energy scale of the RKKY interaction is proportional to Kondo coupling between itinerant electron and localized spin, $k_{\mathrm{B}}T_{\mathrm{RKKY}} \approx J^2\rho(E_F)$ with $\rho(E_{\mathrm{F}})$: density state of free electron at Fermi level. Otherwise, the Kondo temperature is $T_{\mathrm{K}} \approx e^{1/J\rho(E_{\mathrm{F}})}$. The magnetically ordered state is observed for small J, whereas the Kondo effect emerges for its large value [33]. That is the original prototype of quantum phase transition between RKKY magnetic orders (FM or AFM) to Kondo singlet pair due to tuning coupling J.

1.3.2 Non-local magnetic interaction (RKKY)

Many different models are used to explain the magnetic interaction of materials such as strong localization (Heisenberg model), itinerant (RKKY interaction) and superexchange interaction. The Heisenberg model (direct interaction) is used to interpret the emergence of magnetic property of some pure transition elements such as Co, Fe, and Ni, and their compounds. That interaction emerges from strong overlap of two nearest-neighbor magnetic moment orbitals. Otherwise, the Ruderman-Kittel-Kasuya-Yosia interaction was constructed by M. A. Ruderman and C. Kittel to explain the interaction of nuclear magnetic moments at the large distances [29]. Then, D. Kasuya developed the theory to explain that interaction as the second-order perturbation theory in terms of plane wave approximation [19]. Finally, K. Yosia calculated theoretically that model in Cu-Mn alloys to explain emerging of magnetic order by doping Mn impurity on Cu host. They called it as s-d interaction for that magnetic moments interact via conduction electrons.

The RKKY model is one of the most important magnetic interaction prototypes in pure rare-earth elements (Gd, Sm, and Dy) and their alloys. The atomic radius of

rare-earth element (f-shell element) is too large to directly overlap between localized spins of two nearest-neighbor atoms. They would interact indirectly via itinerant electrons. Many other magnetic systems are explained based on RKKY interaction such as heavy fermion materials (the effective mass of metallic compounds is thousands of free electron), diluted magnetic semiconductors (embedded magnetic impurities on semiconductors), Heusler alloys (alloys of non-magnetic elements) and an impurity in graphene. Experimentally, the construction of new advanced technique of spin-resolved scanning tunneling microscopy provide a new method to map the strength and oscillation of RKKY interaction between atoms. Therefore, the derivation of RKKY interaction, is varied from system to system such as spin and charge susceptibilities. However, the main part of RKKY interaction is static Linhard function in the momentum space $\mathbf{q}$ or in the real space $\mathbf{R}$:

$$\chi(\mathbf{q}) = \sum_{\mathbf{k}\in \mathrm{BZ}} \frac{n_F(E_{\mathbf{k}\sigma}) - n_F(E_{\mathbf{k}+\mathbf{q}\sigma})}{E(\mathbf{k}+\mathbf{q}) - E(\mathbf{k})}, \tag{1.14}$$

$$\chi(\mathbf{R}) = \int \frac{(d\mathbf{q})^d}{(2\pi)^d} e^{-i\mathbf{q}\cdot\mathbf{R}} \chi(\mathbf{q}). \tag{1.15}$$

Equation (1.14), $\chi(\mathbf{q})$ in the momentum space Linhard function is calculated over first Brillouin zone (BZ) with $n_F(E_{\mathbf{k}\sigma})$ of the Fermi-Dirac distribution function. The real susceptibility is the Fourier transformation of momentum space with spatial dimensions d. The properties of $\mathbf{q}$-space spin susceptibility is existed of a singular or maximum points which define the order vector of spin interaction. The real space Linhard function $\chi(\mathbf{R})$ is oscillatory and decaying with respect to the distance of two spins. At long range, that function behaves as Bessel function. It is strongly dependent on spatial dimensions d [3].

2D RKKY interaction was computed using plane wave approximation for the metallic energy band. The distance dependence of real spin susceptibility decays as $1/r^2$ for 2D comparing with $1/r^3$ of 3D [14]. RKKY interaction on 2D hexagonal

lattice (graphene) is very attracted to do research because the existence of Dirac points [22, 35]. They demonstrate that the sign-changing oscillation of RKKY in graphene is disappeared due to vanishing of Fermi surface, and the FM state is for magnetic impurities on same sublattice, and AFM for spins on different sublattice [35]. At long distance limit, the RKKY interaction for graphene is r^{-3} decaying rate. The magnetic order of impurity-doped graphene are so controversial. For light doping magnetic impurity at the site of hexagonal lattice, that model develops the AFM order [9, 10]. Otherwise, S. Saremi stated the model of impurity doped graphene is always FM because of semi-metallic properties of graphene [31].

1.3.3 Frustration in magnetic interaction

Frustration plays a important role in strongly correlated electrons and magnetic interactions. In magnetic system, there are two typical types of frustration such as (i) competing between interactions (e.g AFM spin chain) and (ii) geometrical lattices (e.g Kagome lattice and pyrochore lattice). (i) The spins are frustrated in an antiferromagetic chain with considering of the next nearest-neighbor AFM coupling comparing with the nearest coupling [33]. (ii) Kagome lattice has triangular unit cells, if two neighboring spins are interacted antiferromagnetically (oppositely oriented), the direction of third spin at the vertex of triangle cannot be selected to satisfy the AFM coupling of both neighbor spins.

Due to non-local properties of RKKY interaction, it is a potential candidate to explain a frustrating effect and spin glass. For example, J. H. She and his colleagues recently explained the suppressing the magnetic order of the lattice spin by frustration. That interaction leads to the first-order phase transition between magnetic order and spin glass [32]. Furthermore, the RKKY interaction is one of the the best model for interpreting the "spin ice" phenomena in metallic $Pr_2Ir_2O_7$ compounds. The rare-earth Pr^{3+} ions in those compounds form perfect Ising spins with in and out pointing of

tetragona along the local $\langle 111 \rangle$ axis. Those Pr^{3+} Ising spins are interacted via itinerant electron of $5d^5$ Ir^{4+} ions to generate FM coupling. This is the "spin ice" phenomenon for Pr-Pr sublattice [15, 23].

1.4 Motivation

Novel properties of 2D lattice such as graphene and cuprate CuO_2 plane in high-T_c superconductors, they are so attracted to investigate in detail. Especially, the fascinating practical 2D ferromagnetic layer observed triggers to study toward the real applications in spintronic and magneto-electric devices [18].

The changing of Fermi surface is definitely effected to the interacting ground state. For instance, in Kondo lattice materials, small Fermi surface corresponding to AFM order, and large Fermi sufrace is paramagnetic state or Fermi liquid [12]. Also, the analytical calculation of effective RKKY interaction is changed for different Fermi surfaces [28]. We are wondering about collapsing the Fermi surface of zero-flux to Fermi point in π-flux square lattices. How does it affect to RKKY interaction?

Although there are a lot researches about the model of Ising spin at the link coupling with fermion living at the vertex on square lattice [6, 16, 36], those works focuses on the nearest-neighbor interaction with defined coupling constant J. The analytic form of the interaction between the link variables has never been computed. So, we will use the similar crystal lattice, but we will consider the effective long-range interaction of Ising spin with effect RKKY at the weak coupling limit (variable dependence of spin susceptibility). Therefore, our work intends to distinguish the RKKY interaction on two dimension driven by changing spin from site to link, and Fermi surface.

First, I will show the derivation of tight-binding model of free fermions and coupling between spin and fermions (interaction part) for zero-flux and π-flux lattices.

They are known as the Kondo lattice models. At half-filling, the energy band of two cases are plotted to give the Fermi metallic band of zero-flux and semimetallic Dirac band for π-flux. RKKY interactions between spins at the sites and links of both models are derived using the quantum perturbation theory. The momentum space of effective RKKY interaction are calculated in a whole Brillouin zone using C++ code to provide the eigenvalues and corresponding eigenvectors. The maximum point in eigenvalue spectrum will define the magnetic order vector. The long range interaction of a pair of spins in real space show the oscillatory and decaying properties of Linhard function. However, because of coexistence of nearest-neighbor and next-nearest-neighbor interactions of Ising spin in the zero-flux and π-flux lattices, the frustration is necessary to consider. The main work for effective RKKY interaction is summarized in a flow chart:

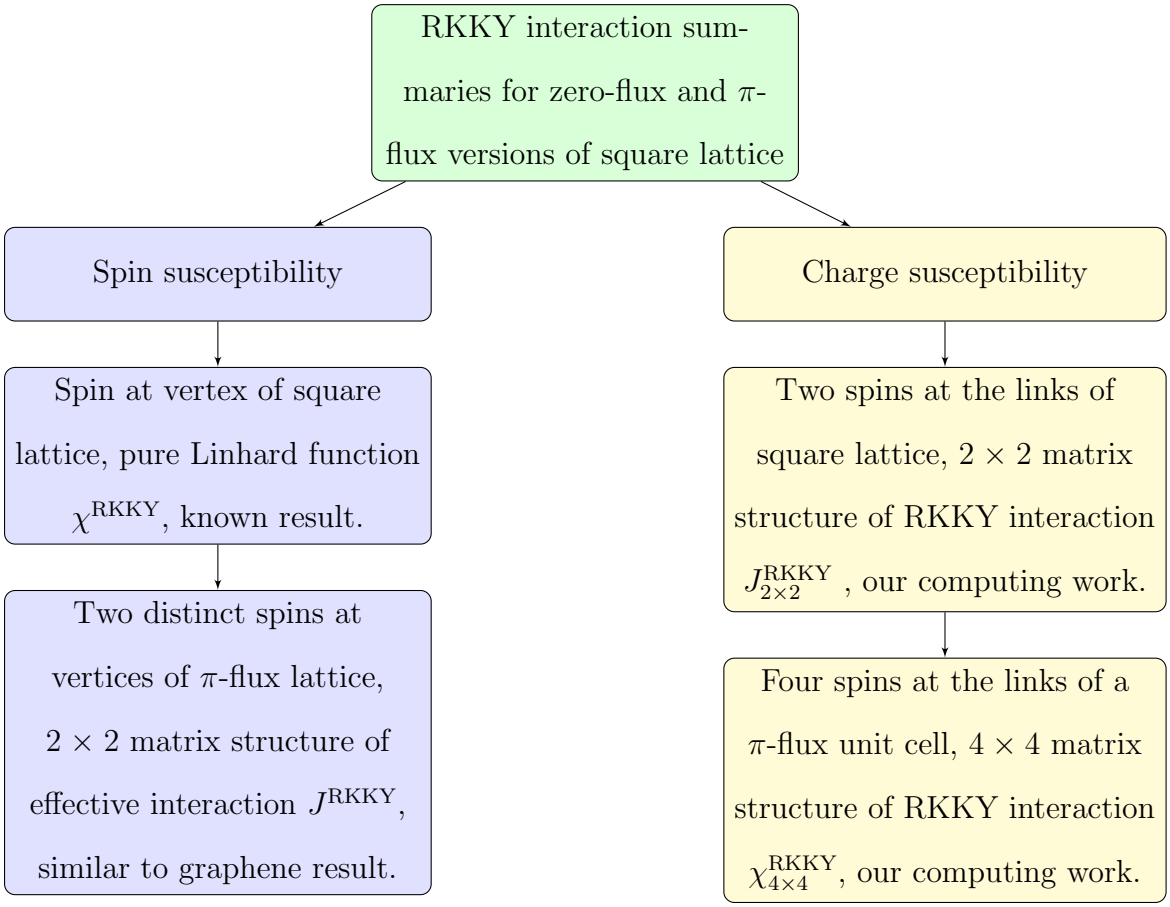

CHAPTER 2

MODELS

2.1 Conventional Fermi Band

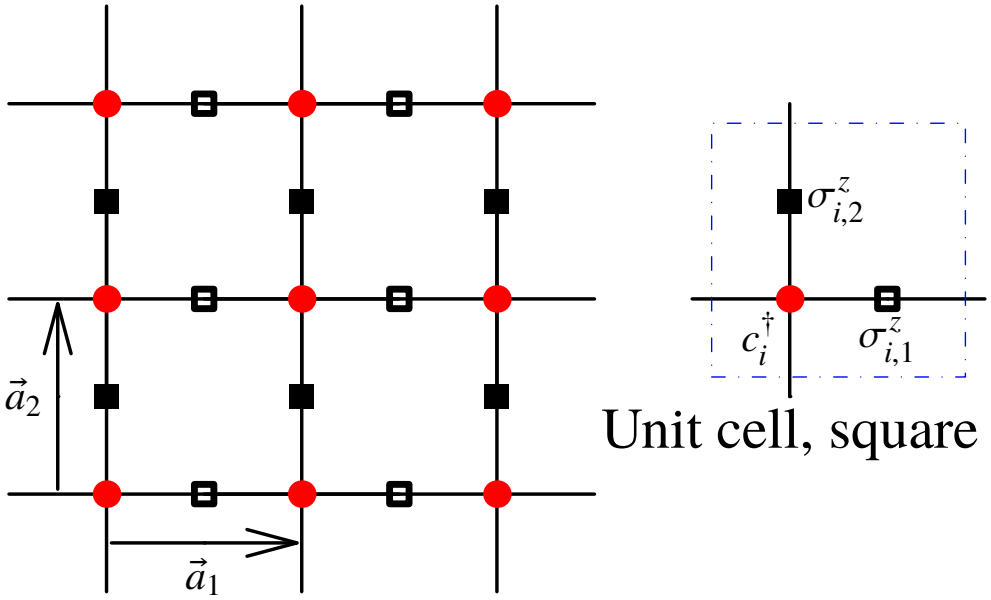

Figure 2.1. The crystal structure of zero-flux square lattice (a case of magnetic field $\mathbf{B} = \mathbf{0}$), and each unit cell consists one fermion $c_i^\dagger$ (fermion basis $\mathbf{b}_\mathrm{f} = (0, 0)$) and two Ising spin $\sigma^z_{i,1}$ (basis $\mathbf{b}_{\mathrm{I}_1} = (1/2, 0)$) distributed along x-direction and $\sigma^z_{i,2}$ (basis $\mathbf{b}_{\mathrm{I}_2} = (0, 1/2)$) arranged along y-direction. Solid line (connects between fermion) illustrates the nearest-neighbor hopping integral $-t$. Lattice vectors are $\mathbf{a}_1 = a(1, 0)$ and $\mathbf{a}_2 = a(0, 1)$, and for simple calculation, we consider lattice constant $a = 1$

In Fig. 2.1, we show the zero-flux square lattice and its arrangement of Ising spins and fermion orbitals. Each unit cell includes one fermion labeled $c^\dagger_{i,\tau}$ (where τ is Pauli spin in z-direction), (we will drop spin index τ for notational simplicity) and Ising spins $\sigma^z_{i,1}$ and $\sigma^z_{i,2}$ are distributed along the x-direction and y-direction, respectively (where i labels the unit cell). Because there are three elements in each unit cell, we

define the basis vectors including $\mathbf{b}_{\mathrm{f}} = (0,0)$ for the fermion, $\mathbf{b}_{\mathrm{I}_1} = (1/2,0)$ for Ising spin 1 (horizontal link), and $\mathbf{b}_{\mathrm{I}_1} = (0,1/2)$ for Ising spin 2 (vertial link). With lattice vectors $\mathbf{a}_1 = (1,0)$ and $\mathbf{a}_2 = (0,1)$, every unit cell of the square lattice can be contructed using translation vector $\mathbf{R} = n\mathbf{a}_1 + m\mathbf{a}_2$ with integers n and m.

The electrons on the vertices of square lattice hop from site to site, and we allows for a nearest-neighbor hopping with amplitude $-t$. That term provides the unperturbed tight-binding Hamiltonian $\hat{H}_0$ in Eq. (2.1). The Ising spins (oriented either up or down) take on values at the link of the square lattice. The coupling constant J between Ising spin and fermion (hopping modulation) gives the interaction part of Hamiltonian $\hat{H}_1$ Eq. (2.1). This term mimics Z_2 Kane-Mele coupling in the spin Hall effect [1]:

$$\begin{aligned}\hat{H} &= \sum_{\langle i,j\rangle}(-t - J\sigma^z_{ij})(c^\dagger_i c_j + c^\dagger_j c_i) = \hat{H}_0 + \hat{H}_1, \\ &= -t\sum_{\langle i,j\rangle}(c^\dagger_i c_j + c^\dagger_j c_i) - J\sum_{\langle i,j\rangle}[\sigma^z_{1,i}(c^\dagger_i c_j + c^\dagger_j c_i) + \sigma^z_{2,i}(c^\dagger_i c_j + c^\dagger_j c_i)].\end{aligned} \tag{2.1}$$

Pairs $\langle i,j\rangle$ denote the nearest-neighbor unit cells. Hamiltonian has the tight-binding with parameter t and interaction parts with parameter J. The t–J model is something else. There are two limits of this model, if $t \gg J$ we can treat the J term as the perturbing part, and vice versa. Because spin and fermion degree of freedoms are admixed, there is no way to diagonalize the full Hamiltonian $\hat{H}$. So, in this work, $\hat{H}_1$ is treated by using perturbation theory. The Hamiltonian is written explicitly in real space with lattice translation vector $\mathbf{R}$:

$$\hat{H}_0 = -t\sum_{\mathbf{R}}[(c^\dagger_{\mathbf{R}+\mathbf{a_1}}c_{\mathbf{R}} + c^\dagger_{\mathbf{R}}c_{\mathbf{R}+\mathbf{a_1}}) + (c^\dagger_{\mathbf{R}+\mathbf{a_2}}c_{\mathbf{R}} + c^\dagger_{\mathbf{R}}c_{\mathbf{R}+\mathbf{a_2}})], \tag{2.2}$$

$$\hat{H}_1 = -J\sum_{\mathbf{R}}[\sigma^z_{1,\mathbf{R}}(c^\dagger_{\mathbf{R}+\mathbf{a_1}}c_{\mathbf{R}} + c^\dagger_{\mathbf{R}}c_{\mathbf{R}+\mathbf{a_1}}) + \sigma^z_{2,\mathbf{R}}(c^\dagger_{\mathbf{R}+\mathbf{a_2}}c_{\mathbf{R}} + c^\dagger_{\mathbf{R}}c_{\mathbf{R}+\mathbf{a_2}})]. \tag{2.3}$$

A better formulation requires us to use Fourier transformation from real space to momentum space both the fermions and Ising spins:

$$c^{\dagger}_{\mathbf{R}} = \frac{1}{\sqrt{N}} \sum_{\mathbf{k}} e^{-i\mathbf{k}.\mathbf{R}} c^{\dagger}_{\mathbf{k}}, \quad (N : \text{number of unit cells}), \tag{2.4}$$

$$\sigma^{z}_{\mathbf{R},\alpha} = \frac{1}{N} \sum_{\mathbf{q}} e^{-i\mathbf{q}.\mathbf{R}} \sigma^{z}_{\mathbf{q},\alpha} \qquad (\text{With} \quad \alpha = 1, 2). \tag{2.5}$$

2.1.1 Non-interacting Hamiltonian

The non-interacting Hamiltonian $\hat{H}_0$ is easily diagonalized to give the energy dispersion relation $E(\mathbf{k})$:

$$\hat{H}_0 = \sum_{\mathbf{k}} E(\mathbf{k}) c^{\dagger}_{\mathbf{k}} c_{\mathbf{k}}, \tag{2.6}$$

$$E(\mathbf{k}) = -2t(\cos k_x + \cos k_y). \tag{2.7}$$

2.1.2 Interacting Hamiltonian

In the momentum basis, the interacting Hamiltonian $\hat{H}_1$ has the following form:

$$\hat{H}_1 = -\frac{J}{N} \sum_{\mathbf{k},\mathbf{q}} \sigma^{z}_{\mathbf{q},1} c^{\dagger}_{\mathbf{k}} c_{\mathbf{k}+\mathbf{q}} \left[e^{-ik_x} + e^{i(k_x+q_x)} \right] + c^{\dagger}_{\mathbf{k}} c_{\mathbf{k}+\mathbf{q}} \sigma^{z}_{\mathbf{q},2} \left[e^{-ik_y} + e^{i(k_y+q_y)} \right]. \tag{2.8}$$

The effective interaction Hamiltonian is constructed from two states:

$$|\Psi_1\rangle = e^{-\hat{H}_0 t} \hat{H}_1 |\Psi_{\text{gs}}\rangle , \tag{2.9}$$

$$|\Psi_2\rangle = \hat{H}_1 e^{-\hat{H}_0 t} |\Psi_{\text{gs}}\rangle . \tag{2.10}$$

State $|\Psi_1\rangle$ is perturbed then evolved in time. State $|\Psi_2\rangle$ is evolved in time then perturbed. Overlapping of two states $|\Psi_1\rangle$ and $|\Psi_2\rangle$ forms the effective interaction

Hamiltonian based on the Heisenberg picture [30]. The ground state is:

$$|\Psi_{\rm gs}\rangle = \prod_{\mathbf{k}<\mathbf{k}_F} c^\dagger_{\mathbf{k}} |0\rangle \quad (\mathbf{k}_F : \text{Fermi wave vector}). \tag{2.11}$$

The effective $\hat{H}_1$ is the second order perturbation in $J << t$. We use Wick's theorem to decompose the four-point correlation function, or charge susceptibility $\chi_c^{\rm RKKY} =$
$\langle\Psi_{\rm gs}| \left[\hat{n}(\mathbf{k},\mathbf{q},t), \hat{n}(\mathbf{k}',\mathbf{q}',t')\right] |\Psi_{\rm gs}\rangle$ (where $\hat{n}(\mathbf{k},\mathbf{q},t) = c^\dagger_{\mathbf{k}}(t) c_{\mathbf{k}+\mathbf{q}}(t)$) in momentum space and Matsubara frequency (Appendix A and B).

The spin susceptibility is written as $\chi_s^{\rm RKKY} = \langle\Psi_{\rm gs}| \left[\mathbf{s}^{\rm a}(\mathbf{k},\mathbf{q},t), \mathbf{s}^{\rm b}(\mathbf{k}',\mathbf{q}',t')\right] |\Psi_{\rm gs}\rangle$ with spins a and b, and itinerant spin $\mathbf{s}^{\rm a}(\mathbf{k},\mathbf{q},t) = \sum_{\alpha\beta} c^\dagger_{\mathbf{k}\alpha} \sigma_{\alpha\beta} c_{\mathbf{k}+\mathbf{q}\beta}$ [32]. Finally, the Linhard function with some momentum correction terms is obtained to give charge susceptibility $J^{\rm RKKY}(\mathbf{q},\omega_n)$ or RKKY interaction between Ising spins. The detail derivation of interacting Hamiltonian is provided in Appendix B.

The final form of $\hat{H}_1$ gives a 2×2 interacting matrix in Matsubara frequency ω_n and two dimensional momentum space k_x and k_y:

$$\hat{H}_1 = -\frac{J^2}{N^2} \sum_{\mathbf{q}} \begin{pmatrix} \sigma^z_{\mathbf{q},1} & \sigma^z_{\mathbf{q},2} \end{pmatrix} J^{\rm RKKY}(\mathbf{q},\omega_n) \begin{pmatrix} \sigma^z_{-\mathbf{q},1} \\ \sigma^z_{-\mathbf{q},2} \end{pmatrix}, \tag{2.12}$$

with the correlation function is given:

$$J^{\rm RKKY}(\mathbf{q},\omega_n) = \sum_{\mathbf{k}} \begin{bmatrix} J_{11}(\mathbf{k},\mathbf{q}) & J_{12}(\mathbf{k},\mathbf{q}) \\ J_{21}(\mathbf{k},\mathbf{q}) & J_{22}(\mathbf{k},\mathbf{q}) \end{bmatrix} \frac{n_F(E_{\mathbf{k}}) - n_F(E_{\mathbf{k}+\mathbf{q}})}{i\omega_n + E_{\mathbf{k}+\mathbf{q}} - E_{\mathbf{k}}}. \tag{2.13}$$

All terms of the charge susceptibility are listed below:

$$J_{11}(\mathbf{k},\mathbf{q}) = 2 + e^{i(2k_x+q_x)} + e^{-i(2k_x+q_x)} = 4\cos^2(k_x + \frac{q_x}{2}), \tag{2.14}$$

$$J_{22}(\mathbf{k},\mathbf{q}) = 2 + e^{i(2k_y+q_y)} + e^{-i(2k_y+q_y)} = 4\cos^2(k_y + \frac{q_y}{2}), \tag{2.15}$$

$$J_{12}(\mathbf{k},\mathbf{q}) = e^{-i(k_x+k_y+q_y)} + e^{i(k_x+k_y+q_x)} + e^{-i(k_x-k_y)} + e^{i(k_x-k_y+q_x-q_y)}, \tag{2.16}$$

$$J_{21}(\mathbf{k},\mathbf{q}) = e^{i(k_x+k_y+q_y)} + e^{-i(k_x+k_y+q_x)} + e^{i(k_x-k_y)} + e^{-i(k_x-k_y+q_x-q_y)}, \tag{2.17}$$

$$n_F(E_\mathbf{k}) = \frac{1}{e^{\beta(E_\mathbf{k}-\mu)}+1}, \tag{2.18}$$

where $n_F(E_\mathbf{k})$ is Fermi-Dirac distribution function. The half-filling case corresponds to chemical potential $\mu = 0$ (each site is occupied by exact one fermion).

2.2 Dirac Band

Figure 2.2 shows the π-flux square lattice with decorating of fermions and Ising spins. A unit cell of π-flux is doubled zero-flux one. It consists of two fermions labeling $c^\dagger_{i,\mathrm{A}}$ and $c^\dagger_{i,\mathrm{B}}$ are arranged at the vertices (in the figure 2.2). Four Ising spins $\sigma^z_{i,1}$, $\sigma^z_{i,2}$, $\sigma^z_{i,3}$ and $\sigma^z_{i,4}$ are put at the middle of each link. The two lattice vectors are $\mathbf{a}'_1 = \mathbf{a}_1$ and $\mathbf{a}'_2 = 2\mathbf{a}_2$ ($\mathbf{a}_1$ and $\mathbf{a}_2$ are lattice vectors of zero-flux). The hopping integral of π-flux lattice is two values. The nearest neighbor hopping between fermion B–B is $+t$ (dotted line in Fig. 2.2), and other hopping integrals of A–A, B–A and A–B are $-t$ (solid line). The coupling between fermion and Ising spins are J. Hamiltonian of this model is formulated:

$$\hat{H} = \sum_{\langle i,j\rangle}(-t_{ij} - J_{ij}\sigma_{ij})(c^\dagger_i c_j + c^\dagger_j c_i) = \hat{H}_0 + \hat{H}_1, \tag{2.19}$$

$$\hat{H} = \sum_{\langle i,j\rangle} t_{ij}(c^\dagger_i c_j + c^\dagger_j c_i) + \sum_{\langle i,j\rangle,\alpha} J_{ij}\sigma_{ij,\alpha}(c^\dagger_i c_j + c^\dagger_j c_i), \tag{2.20}$$

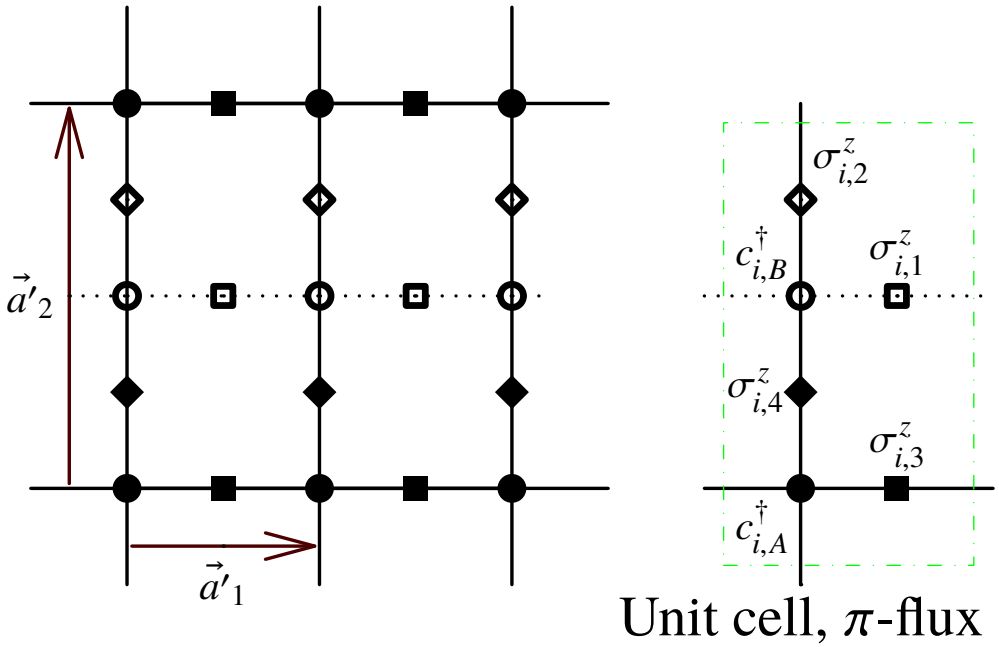

Figure 2.2. The crystal structure of π-flux lattice (magnetic field $\mathbf{B} \neq \mathbf{0}$), and each unit cell is doubled in size of zero-flux. It includes 2 distinct fermions $c^\dagger_{i,A}$ (basis $\mathbf{b}'_{\mathrm{A}} = (0,0)$) (distributed along solid line) and $c^\dagger_{i,B}$ (basis $\mathbf{b}'_{\mathrm{B}} = (0,1)$) (arranged along dotted line) and 4 Ising spins such as $\sigma^z_{i,1}$ (basis $\mathbf{b}'_{\mathrm{I}_1} = (1/2,1)$), $\sigma^z_{i,2}$ (basis $\mathbf{b}'_{\mathrm{I}_2} = (0,3/2)$), $\sigma^z_{i,3}$ (basis $\mathbf{b}'_{\mathrm{I}_3} = (1/2,0)$)and $\sigma^z_{i,4}$ (basis $\mathbf{b}'_{\mathrm{I}_4} = (0,1/2)$). Solid lines show hopping integral $-t$, and dotted lines mean $+t$ hopping integral. Two lattice vectors are $\mathbf{a}'_1 = (1,0)$ and $\mathbf{a}'_2 = (0,2)$

with $\alpha = 1,\ 2,\ 3,$ and 4, and $\langle i,j \rangle$ is the nearest-neighbor of unit cell. The full Hamiltonian separates into tight binding part $\hat{H}_0$ and interaction part $\hat{H}_1$ with small perturbation coefficient J. The explicit form $\hat{H}$ with vector $\mathbf{R}$ in real space:

$$\begin{aligned}
\hat{H} \;=\; \sum_{\mathbf{R}} \Big[& -(t + J\sigma^z_{\mathbf{R},2}) c^\dagger_{\mathbf{R}+\mathbf{a}_2,\mathrm{A}} c_{\mathbf{R},\mathrm{B}} \\
& + (t - J\sigma^z_{\mathbf{R},1}) c^\dagger_{\mathbf{R}+\mathbf{a}_1,\mathrm{B}} c_{\mathbf{R},\mathrm{B}} + (t - J\sigma^z_{\mathbf{R}-\mathbf{a}_1,1}) c^\dagger_{\mathbf{R}+\mathbf{a}_1,\mathrm{B}} c_{\mathbf{R},\mathrm{B}} \\
& - (t + J\sigma^z_{\mathbf{R},4})(c^\dagger_{\mathbf{R},\mathrm{B}} c_{\mathbf{R},\mathrm{A}} + c^\dagger_{\mathbf{R},\mathrm{A}} c_{\mathbf{R},\mathrm{B}}) - (t - J\sigma^z_{\mathbf{R},3}) c^\dagger_{\mathbf{R}+\mathbf{a}_1,\mathrm{A}} c_{\mathbf{R},\mathrm{A}} \\
& - (t - J\sigma^z_{\mathbf{R}-\mathbf{a}_1,3}) c^\dagger_{\mathbf{R}-\mathbf{a}_1,\mathrm{A}} c_{\mathbf{R},\mathrm{A}} - (t + J\sigma^z_{\mathbf{R}-\mathbf{a}_2,2}) c^\dagger_{\mathbf{R}-\mathbf{a}_2,\mathrm{B}} c_{\mathbf{R},\mathrm{B}} \Big]. \qquad (2.21)
\end{aligned}$$

2.2.1 Unperturbed Hamiltonian

$$\begin{aligned}\hat{H}_0 &= \sum_{\mathbf{R}} \big[-t(c^{\dagger}_{\mathbf{R}+\mathbf{a}_2,\mathrm{A}} c_{\mathbf{R},\mathrm{B}} + c^{\dagger}_{\mathbf{R}-\mathbf{a}_2,\mathrm{B}} c_{\mathbf{R},\mathrm{A}}) + t(c^{\dagger}_{\mathbf{R}+\mathbf{a}_1,\mathrm{B}} c_{\mathbf{R},\mathrm{B}} + c^{\dagger}_{\mathbf{R}-\mathbf{a}_1,\mathrm{B}} c_{\mathbf{R},\mathrm{B}}) \\ &\quad - t(c^{\dagger}_{\mathbf{R},\mathrm{B}} c_{\mathbf{R},\mathrm{A}} + c^{\dagger}_{\mathbf{R},\mathrm{A}} c_{\mathbf{R},\mathrm{B}}) - t(c^{\dagger}_{\mathbf{R}+\mathbf{a}_1,\mathrm{A}} c_{\mathbf{R},\mathrm{A}} + c^{\dagger}_{\mathbf{R}+\mathbf{a}_1,\mathrm{A}} c_{\mathbf{R},\mathrm{A}}) \big]. \end{aligned} \tag{2.22}$$

First, using discrete Fourier transformations between real and momentum space, the unperturbed Hamiltonian $\hat{H}_0$ is written as a 2×2 matrix in the sublattice structure (Eq. (2.25)). With $H_{\mathbf{k}}$ (Eq. (2.26)) is called the kernel of $\hat{H}_0$.

$$c^{\dagger}_{\mathbf{R},\mathrm{A/B}} = \frac{1}{\sqrt{N}} \sum_{\mathbf{k}} e^{-i\mathbf{k}.\mathbf{R}} c^{\dagger}_{\mathbf{k},\mathrm{A/B}} \quad (N\text{: number of unit cell}), \tag{2.23}$$

$$\sigma^{z}_{\mathbf{R},\alpha} = \frac{1}{N} \sum_{\mathbf{q}} e^{-i\mathbf{q}.\mathbf{R}} \sigma^{z}_{\mathbf{q},\alpha} \quad (\alpha = 1,2,3,4), \tag{2.24}$$

$$\hat{H}_0 = -t \sum_{\mathbf{k}} \begin{pmatrix} c^{\dagger}_{\mathbf{k},\mathrm{A}} & c^{\dagger}_{\mathbf{k},\mathrm{B}} \end{pmatrix} H_{\mathbf{k}} \begin{pmatrix} c_{\mathbf{k},\mathrm{A}} \\ c_{\mathbf{k},\mathrm{B}} \end{pmatrix}, \tag{2.25}$$

$$H_{\mathbf{k}} = \begin{bmatrix} 2\cos(k_x a) & 1 + e^{-i\mathbf{k}.\mathbf{a}_2} \\ 1 + e^{i\mathbf{k}.\mathbf{a}_2} & -2\cos(k_x a) \end{bmatrix}. \tag{2.26}$$

After diagonalization $\hat{H}_0$, the energy dispersion relations $E_{2,1}(\mathbf{k})$ which are corresponding to upper part and lower Dirac bands are achieved in Eq. (2.27). Also, quasiparticle basis are constructed with new creation and annihilation operators $f_{\mathbf{k},2}$, $f^{\dagger}_{\mathbf{k},2}$, $f_{\mathbf{k},1}$ and $f^{\dagger}_{\mathbf{k},1}$.

$$E_{2,1}(\mathbf{k}) = \pm 2t \sqrt{\cos {k_x}^2 + \cos {k_y}^2}. \tag{2.27}$$

And the diagonalized Hamiltonian $\hat{H}_0$ is written in term of new basis:

$$\begin{aligned}\hat{H}_0 &= \sum_{\mathbf{k}} \left[E_2(\mathbf{k}) f^\dagger_{\mathbf{k},2} f_{\mathbf{k},2} + E_1(\mathbf{k}) f^\dagger_{\mathbf{k},1} f_{\mathbf{k},1}\right] \\ &= \sum_{\mathbf{k}} 2t\sqrt{\cos^2 k_x + \cos^2 k_y}\left(f^\dagger_{\mathbf{k},2} f_{\mathbf{k},2} - f^\dagger_{\mathbf{k},1} f_{\mathbf{k},1}\right).\end{aligned} \tag{2.28}$$

Unitary matrices $U_{2\times2}$ and $U^\dagger_{2\times2}$ transform from fermion basis $c^\dagger_{\mathbf{k},\mathrm{A/B}}$ and $c_{\mathbf{k},\mathrm{A/B}}$ to $f_{\mathbf{k},2}$, $f^\dagger_{\mathbf{k},2}$, $f_{\mathbf{k},1}$ and $f^\dagger_{\mathbf{k},1}$ quasiparticle basis.

$$U_{2\times2} = \frac{1}{\beta(\mathbf{k})}\begin{bmatrix} \frac{1+e^{-2ik_y}}{2} & \frac{-1-e^{2ik_y}}{2} \\ \alpha(\mathbf{k}) & \alpha(\mathbf{k}) \end{bmatrix}, \tag{2.29}$$

$$U^\dagger_{2\times2} = \frac{1}{\beta(\mathbf{k})}\begin{bmatrix} \frac{1+e^{2ik_y}}{2} & \alpha(\mathbf{k}) \\ \frac{-1-e^{-2ik_y}}{2} & \alpha(\mathbf{k}) \end{bmatrix}. \tag{2.30}$$

There are number of supplemental functions in unitary matrices:

$$\alpha(\mathbf{k}) = \sqrt{\cos^2 k_x + \cos^2 k_y} - \cos k_x, \tag{2.31}$$

$$\beta(\mathbf{k}) = \sqrt{2(\cos^2 k_x + \cos^2 k_y - \cos k_x\sqrt{\cos^2 k_x + \cos^2 k_y})}, \tag{2.32}$$

$$\alpha(\mathbf{k},\mathbf{q}) = \sqrt{\cos^2(k_x+q_x) + \cos^2(k_y+q_y)} - \cos(k_x+q_x), \tag{2.33}$$

$$\beta(\mathbf{k},\mathbf{q}) = \sqrt{2[\cos^2(k_x+q_x) + \cos^2(k_y+q_y) - \cos(k_x+q_x)\sqrt{\cos^2(k_x+q_x) + \cos^2(k_y+q_y)}]}. \tag{2.34}$$

2.2.2 RKKY interaction

$$\begin{aligned}\hat{H}_1 &= -J\sum_{\mathbf{R}}\big[\sigma^z_{\mathbf{R},2}c^\dagger_{\mathbf{R}+\mathbf{a}_2,\mathrm{A}}c_{\mathbf{R},\mathrm{B}}+\sigma^z_{\mathbf{R}-\mathbf{a}_2,2}c^\dagger_{\mathbf{R}-\mathbf{a}_2,\mathrm{B}}c_{\mathbf{R},\mathrm{A}}\\ &\quad+\sigma^z_{\mathbf{R},1}c^\dagger_{\mathbf{R}+\mathbf{a}_1,\mathrm{B}}c_{\mathbf{R},\mathrm{B}}+\sigma^z_{\mathbf{R}-\mathbf{a}_1,1}c^\dagger_{\mathbf{R}-\mathbf{a}_1,\mathrm{B}}c_{\mathbf{R},\mathrm{B}}+\sigma^z_{\mathbf{R},4}(c^\dagger_{\mathbf{R},\mathrm{B}}c_{\mathbf{R},\mathrm{A}}+c^\dagger_{\mathbf{R},\mathrm{A}}c_{\mathbf{R},\mathrm{B}})\\ &\quad-\sigma^z_{\mathbf{R},3}c^\dagger_{\mathbf{R}+\mathbf{a}_1,\mathrm{A}}c_{\mathbf{R},\mathrm{A}}-\sigma^z_{\mathbf{R}-\mathbf{a}_1,3}c^\dagger_{\mathbf{R}-\mathbf{a}_1,\mathrm{A}}c_{\mathbf{R},\mathrm{A}}\big]. \qquad (2.35)\end{aligned}$$

The derivation of RKKY interaction for π-flux lattice is similar to conventional Fermi band. We will construct 2 states $|\Psi_1\rangle$ and $|\Psi_2\rangle$ and take their overlaps to get the effective Hamiltonian (detailed derivation is showed in Appendix A). The charge susceptibility of effective Hamiltonian $\hat{H}_1$ provides in 4×4 matrix with common Linhard function:

$$\hat{H}_1 = -\frac{J^2}{N^2}\sum_{\mathbf{q}}\begin{pmatrix}\sigma^z_{\mathbf{q},1} & \sigma^z_{\mathbf{q},2} & \sigma^z_{\mathbf{q},3} & \sigma^z_{\mathbf{q},4}\end{pmatrix}\chi^{\mathrm{RKKY}}_{4\times4}(\mathbf{q},\omega_n)\begin{pmatrix}\sigma^z_{-\mathbf{q},1}\\ \sigma^z_{-\mathbf{q},2}\\ \sigma^z_{-\mathbf{q},3}\\ \sigma^z_{-\mathbf{q},4}\end{pmatrix} \qquad (2.36)$$

$$\chi^{\mathrm{RKKY}}_{4\times4}(\mathbf{q},\omega_n) = \sum_{\mathbf{k}}M_{4\times4}(\mathbf{k},\mathbf{q})\frac{n_F(E_{\mathbf{k},1})-n_F(E_{\mathbf{k}+\mathbf{q},2})}{i\omega_n+E_{\mathbf{k}+\mathbf{q},2}-E_{\mathbf{k},1}}, \qquad (2.37)$$

$$M_{4\times4}(\mathbf{k},\mathbf{q}) = \begin{bmatrix}M_{11}(\mathbf{k},\mathbf{q}) & M_{12}(\mathbf{k},\mathbf{q}) & M_{13}(\mathbf{k},\mathbf{q}) & M_{14}(\mathbf{k},\mathbf{q})\\ M_{21}(\mathbf{k},\mathbf{q}) & M_{22}(\mathbf{k},\mathbf{q}) & M_{23}(\mathbf{k},\mathbf{q}) & M_{24}(\mathbf{k},\mathbf{q})\\ M_{31}(\mathbf{k},\mathbf{q}) & M_{32}(\mathbf{k},\mathbf{q}) & M_{33}(\mathbf{k},\mathbf{q}) & M_{34}(\mathbf{k},\mathbf{q})\\ M_{41}(\mathbf{k},\mathbf{q}) & M_{42}(\mathbf{k},\mathbf{q}) & M_{43}(\mathbf{k},\mathbf{q}) & M_{44}(\mathbf{k},\mathbf{q})\end{bmatrix}. \qquad (2.38)$$

All elements of matrix $M_{4\times4}(\mathbf{k},\mathbf{q})$ are listed in the appendix A.

CHAPTER 3

RESULTS AND DISCUSSION

3.1 Fermi band and Dirac band

3.1.1 Brillouin zone

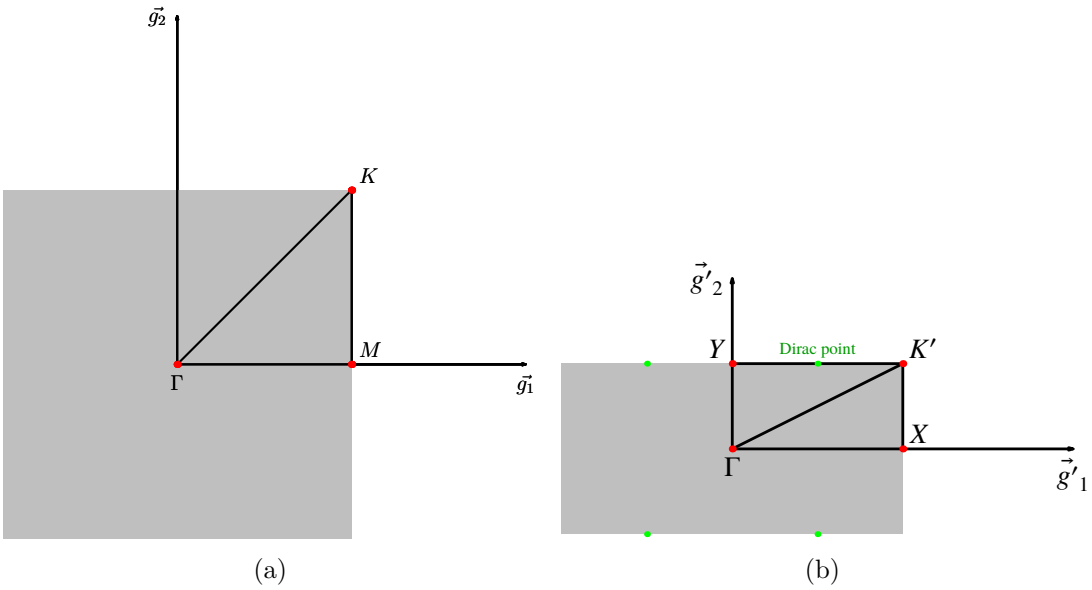

Figure 3.1. The first Brillouin zone of square lattice for (a) zero-flux and (b) π-flux (gray color).

Figure 3.1 shows the first Brillouin zone (gray color region) of square lattice threaded with (a) zero-flux (magnetic field $\mathbf{B} = \mathbf{0}$) and (b) π-flux (magnetic field $\mathbf{B} \neq \mathbf{0}$). In Fig. 3.1(a), the first Brillouin zone of zero-flux square lattice is constructed from two reciprocal vectors $\mathbf{g}_1 = (2\pi, 0)$ and $\mathbf{g}_2 = (0, 2\pi)$ [5]. Some high-symmetry points are $\Gamma = (0, 0)$, M $= (\pi, 0)$ and K $= (\pi, \pi)$ in that zone.

Figure 3.1(b) shows the rectangular shape of the first Brillouin zone for π-flux lattice. The reciprocal vectors of π-flux are $\mathbf{g}'_1 = \mathbf{g}_1$ and $\mathbf{g}'_2 = \frac{1}{2}\mathbf{g}_2$. Because of

asymmetrical Brillouin zone, we consider more points such as $\Gamma = (0, 0)$, $\mathrm{X} = (\pi, 0)$, $\mathrm{K}' = (\pi, \frac{\pi}{2})$, and $\mathrm{Y} = (0, \frac{\pi}{2})$. The four green dots represent the Dirac points at Brillouin zone, where upper and bands of energy dispersion relation contact each other. Because of different Brillouin zones, the properties of zero-flux and π-flux square lattices will be different.

3.1.2 Energy dispersion relation for square and π-flux lattices

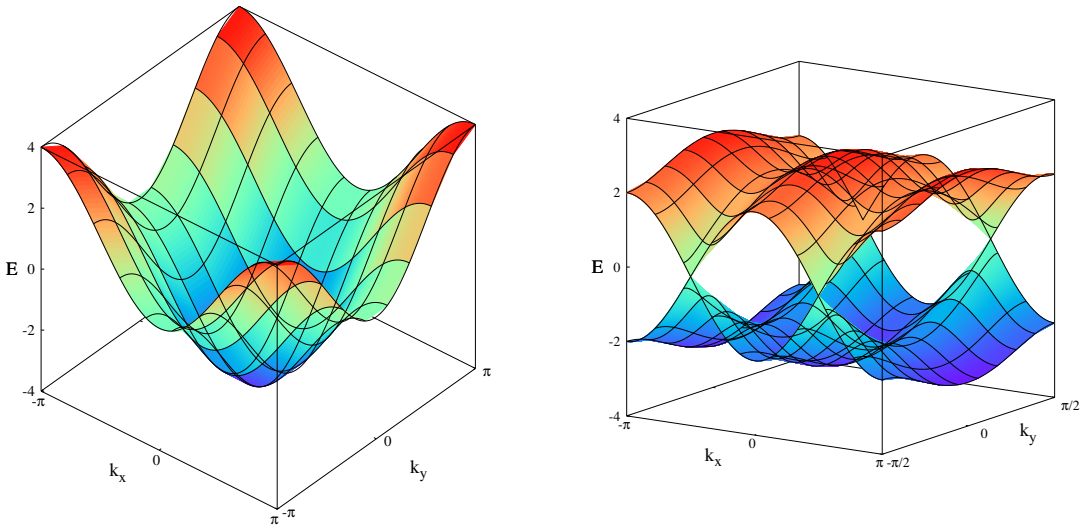

(a) (b)

Figure 3.2. 3 dimensional surfaces of (a) zero-flux square lattice with energy dispersion $E = -2t(\cos k_x + \cos k_y)$, and (b) π-flux lattice with energy dispersion $E_{2/1} = \pm 2t\sqrt{(\cos^2 k_x + \cos^2 k_y)}$ (with hopping integral $t = 1$)

Figures 3.2 and 3.3 exhibit conventional Fermi band of zero-flux and Dirac bands of π-flux lattices. Figures 3.2(a) and 3.3(a) show 3D surface and 2D contour plots of energy dispersion $E = -2t(\cos k_x + \cos k_y)$ $(t = 1)$. The continuous energy dispersion of zero-flux lattice illustrates a metallic band. At the half-filling, each site of lattice is occupied exactly one electron. The Fermi surface is a diamond (red line in Fig. 3.3(a)) with Fermi energy $E_F = 0$. The Fermi surface of square lattice has a nesting property. There is an existence of vector $\mathbf{Q}_0 = (\pm\pi, \pm\pi)$, nesting vectors

which connect all points on Fermi surface [33]. This property will strongly affect to the interaction of spin, discuss next section.

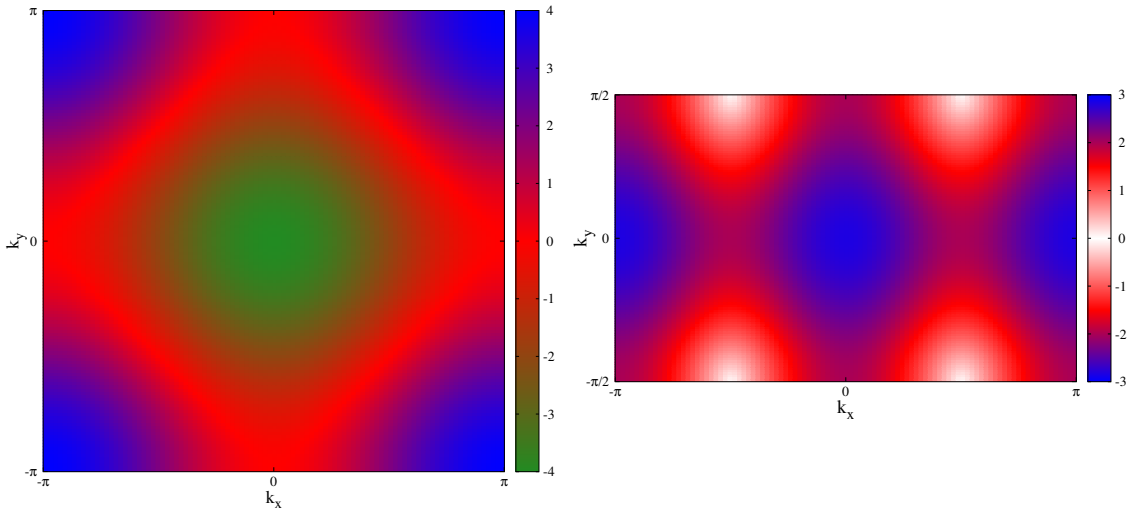

(a) (b)

Figure 3.3. Two dimensional contour plots of (a) zero-flux square lattice with energy dispersion $E = -2t(\cos k_x + \cos k_y)$, and (b) π-flux lattice with energy dispersion $E_{2/1} = \pm 2t\sqrt{(\cos^2 k_x + \cos^2 k_y)}$ (with hopping integral $t = 1$)

Figures 3.2(b) and 3.3(b) show the 3D surface and 2D contour plots of energy dispersion $E_{2,1} = \pm 2t\sqrt{\cos^2 k_x + \cos^2 k_y}$ (the value of hopping integral $t = 1$). There are upper E_2 and lower E_1 bands. They touches each other at four Dirac points $(k_x = \pm\frac{\pi}{2}, k_y = \pm\frac{\pi}{2})$ (white region in the Fig. 3.3(b)). At the half-filling, the Fermi surface collapses to Fermi points [27]. So, the upper band E_2 is empty state (a electron band), and lower band E_1 is completely filled, hole band. That is a typical band structure of semi-metal (e.g graphene [25]).

3.2 RKKY interaction in zero-flux lattice

RKKY interaction for spin in "site model"

First, let's look at the standard RKKY interaction of conventional zero-flux square lattice, shown in Eq. (3.1). For that model, each vertex is put an magnetic im-

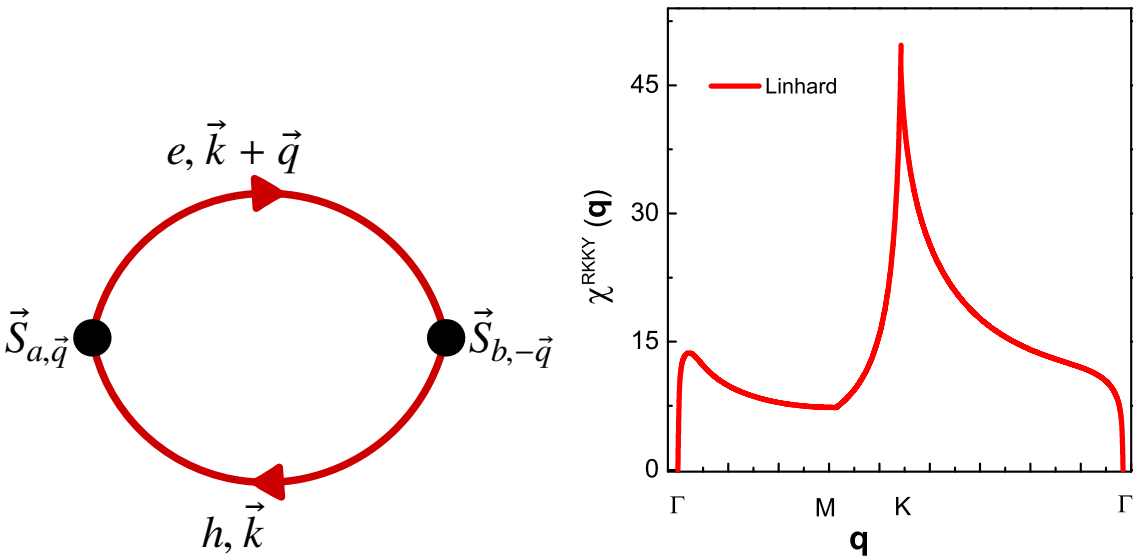

(a) (b)

Figure 3.4. (a) Particle-hole symmetry structure which is driven magnetic mechanism of spins, and (b) the pure Linhard function versus momentum vector $\chi^{\mathrm{RKKY}}(\mathbf{q})$ along Γ–M–K–Γ in square Brillouin zone (Γ = $(0,0)$, M = $(\pi,0)$ and K = (π,π) in Fig. 3.1(a))

purity, spin $\mathbf{S}$ (considering $\mathbf{S} = \frac{1}{2}$ spin for this case), this is typical spin susceptibility of "site model" [33]. RKKY interaction of that model is the pure Linhard function $\chi^{\mathrm{RKKY}}(\mathbf{q}, \omega_n)$. Following Fermi liquid theory [5, 33], the nonlocal magnetic interaction of 2 spins is driven by particle-hole symmetry (Fig. 3.4(a)). Due to interacting excitation, a hole with momentum vector $\mathbf{k}$ is created below the Fermi surface, and electron with $\mathbf{k}+\mathbf{q}$ is above the Fermi surface [33]. One spin $\mathbf{S}_{a,\mathbf{q}}$ coupling with electron interacts with spin $\mathbf{S}_{b,-\mathbf{q}}$ which is coupling with hole. That symmetry is related to the polarization of electrons around the Fermi surface [22]. The particle-hole symmetry is intraband and interband transitions in Fermi, Dirac bands, respectively.

Figure 3.4(b) shows the plot of Linhard function $\chi^{\mathrm{RKKY}}(\mathbf{q}, \omega_n)$ with respect to momentum $\mathbf{q}$ along Γ–M–K–Γ path (Γ = $(0,0)$, M = $(\pi,0)$ and K = (π,π) in Fig. 3.1(a)). That function is minimum at points Γ = $(0,0)$, and maximum singularity at points K = (π,π). According to the result of J. H. She *et al.*, the ordering vector

of magnetic interaction is defined at the point which is the maximum singularity of $\chi^{\mathrm{RKKY}}(\mathbf{q})$ function. That is due to that maximum value with minus sign of coupling constant $\frac{-J^2}{N^2}$ gives the minimum magnetic energy (stable system) [32]. Magnetic pattern of that model is known as alternative 2D AFM (type-G AFM, Fig.14.3 of ref.[33]). To make a compare and contrast with Ising spin "link model" for zero-flux lattice, we draw "site model" in Fig. 3.7(a).

$$H_{\mathrm{RKKY}} = \frac{-J^2}{N^2} \sum_{\mathbf{k}} \chi^{\mathrm{RKKY}}(\mathbf{q}, \omega_n) \mathbf{S}(\mathbf{q}) \cdot \mathbf{S}(-\mathbf{q}), \tag{3.1}$$

$$\chi^{\mathrm{RKKY}}(\mathbf{q}, \omega_n) = \sum_{\mathbf{k} \in BZ} \frac{n_F(E_{\mathbf{k}}) - n_F(E_{\mathbf{k}+\mathbf{q}})}{i\omega_n + E_{\mathbf{k}+\mathbf{q}} - E_{\mathbf{k}}}. \tag{3.2}$$

RKKY interaction for Ising spin in "link model"

Equation 2.12 show the 2×2 matrix charge susceptibility of $\hat{H}_1$ includes the interaction of Ising spin σ_1^z and σ_1^z (labeled Ising 1-1), Ising spin σ_1^z and σ_2^z (Ising 1-2) and Ising spin σ_2^z and σ_2^z (Ising 2-2). Because of symmetric property, interaction between Ising spin σ_1^z and σ_1^z is similar to σ_2^z and σ_2^z. The typical Linhard part $\chi(\mathbf{q}, \omega_n)$ is driven of interaction (Eq. 3.3).

In order to determine magnetic order of Ising spins, we compute charge susceptibility $J_{2\times2}^{\mathrm{RKKY}}$ in momentum space and real space. In momentum space, the $J_{2\times2}^{\mathrm{RKKY}}(\mathbf{q})$ function is calculated using quadrature integral method for the whole Brillouin zone. We divide k_x and k_y from $-\pi$ to π into N intervals, and $N = L_x = L_y$ (L_x and L_y are the lengths of real lattice). For Matsubara frequency $\omega_n = (2n+1)T$, we select temperature $T = 0.01$ K and $n = 0$. 2×2 matrix is diagonalized to give 2 eigenvalues such as $Eigen1$ and $Eigen2$ (Fig. 3.5). Finally, they are plotted along a Γ–M–K–Γ

path ($\Gamma = (0,0)$, $M = (\pi, 0)$ and $K = (\pi, \pi)$ in figure 3.1(a)).

$$J^{\mathrm{RKKY}}_{2\times 2}(\mathbf{q}, \omega_n) = \int_{-\pi}^{\pi}\int_{-\pi}^{\pi} \frac{dk_x dk_y}{(2\pi)^2} \begin{bmatrix} J_{11}(\mathbf{k},\mathbf{q}) & J_{12}(\mathbf{k},\mathbf{q}) \\ J_{21}(\mathbf{k},\mathbf{q}) & J_{22}(\mathbf{k},\mathbf{q}) \end{bmatrix} \frac{n_F(E_{\mathbf{k}}) - n_F(E_{\mathbf{k+q}})}{i\omega_n + E_{\mathbf{k+q}} - E_{\mathbf{k}}}. \tag{3.3}$$

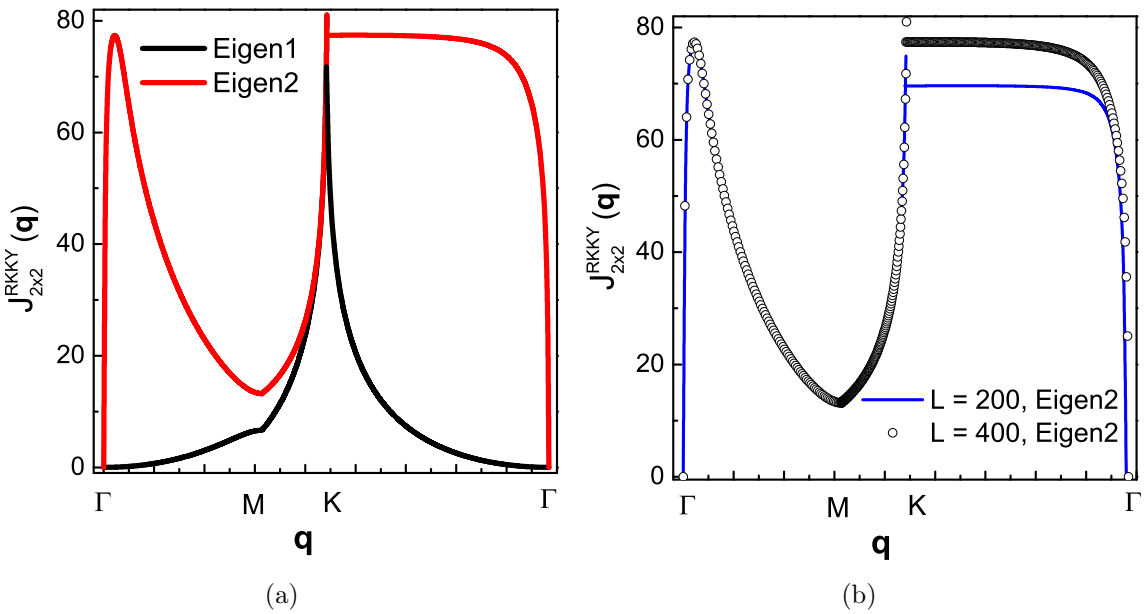

Figure 3.5. RKKY interaction versus momentum vector $J^{\mathrm{RKKY}}_{2\times 2}(\mathbf{q})$ with two eigenvalues *Eigen*1 and *Eigen*2 (lattice size $L = 400$), and (b) *Eigen*2 with different lattice sizes ($L = 200,\ 400$) in Γ–M–K–Γ path of square Brillouin zone (with $\Gamma = (0,0)$, $\mathrm{M} = (\pi, 0)$, and $\mathrm{K} = (\pi, \pi)$)

Figure 3.5(a) shows the two eigenvalues of $J^{\mathrm{RKKY}}_{2\times 2}(\mathbf{q})$ function along the Γ–M–K–Γ path. *Eigen*1 and *Eigen*2 curves are distinct shapes. The *Eigen*1 curve is similar to spin susceptibility $\chi^{\mathrm{RKKY}}(\mathbf{q})$ of "site model", while *Eigen*2 one is different. However, they have a same singular point of $\mathrm{K} = (\pi, \pi)$. To clarify singularity, we plot the *Eigen*2 for different lattice sizes with $L = 200$, and 400 (Fig. 3.5(b)). By increasing lattice size, the singular point is sharper.

Due to the symmetrical property, other singularities are $(-\pi,\ \pi)$ and $(\pi, -\pi)$ and $(-\pi, -\pi)$ which are the vertices of Fermi surface (red diamond of Brillouin zone in Fig. 3.3(a)). Those ordering magnetic vectors are strongly commensurate to the

nesting wave vectors $\mathbf{Q}_0 = (\pm\pi, \pm\pi)$. Jenő Sólyom stated that Linhard function is singular at the nesting vector $\mathbf{Q}_0$ because of the energy dispersion $E_{\mathbf{k}} = E_{\mathbf{k}+\mathbf{Q}_0}$ which provides its denominator zero value [33]. The nesting of Fermi surface is as strong as to preserve the property of singularity in both cases of "site model" and "link model" of zero-flux square lattice.

However, for the "link model", the RKKY interaction is more complicated because of existence of two Ising spins σ_1^z and σ_2^z. The eigenvector are also carried out to know about the magnetic wave vector. At the $K = (\pi, \pi)$ point, eigenvector V_1 of $Eigen1$ defines ferromagnetic (FM) interaction, and eigenvector V_2 of $Eigen2$ defines AFM order (Eq.3.4). Since the singular peak of $Eigen2$ is higher than $Eigen1$ one, the AFM order will dominate with ordering wave vector $\mathbf{Q}_o = (\pi, \pi)$.

$$V_1 = \frac{1}{\sqrt{2}} \begin{pmatrix} -1 \\ -1 \end{pmatrix} \qquad V_2 = \frac{1}{\sqrt{2}} \begin{pmatrix} 1 \\ -1 \end{pmatrix} \tag{3.4}$$

To define exact AFM for that model, the real space of charge susceptibility $J_{\alpha\beta}^{\mathrm{RKKY}}(\mathbf{R})$ (with $\mathbf{R} = \mathbf{R}_j - \mathbf{R}_i$: distance vector of two unit cell i and j) is calculated by using discrete Fourier transformation of momentum $J_{\alpha\beta}^{\mathrm{RKKY}}(\mathbf{q})$ (Eq. (3.5)). The interaction of Ising 1-1 $J_{11}^{\mathrm{RKKY}}(\mathbf{R})$ follow Eq. (3.5) with two unit cells i and j, and $\alpha = 1$ and $\beta = 1$. Figure 3.6(a) shows the plot of function $J_{11}^{\mathrm{RKKY}}(\mathbf{R})$ for "link model" comparing with spin susceptibility $\chi^{\mathrm{RKKY}}(\mathbf{R})$ of "site model" for unit cells i and j in x-direction. Both two functions decays so fast with respect to the distance $R = |\mathbf{R}|$ strong agreement with the result of RKKY interaction in 2D case [3].

Inset of figure 3.6(a) rooms in the short range interaction of two model within 10 unit cell. The Ising spins strongly interact each other in the range of 5-6 unit cells. In contrast to sign-changed oscillation (black circle) of RKKY interaction of "site model", there is no changing sign of charge susceptibility of Ising 1-1 (red half-filled square).

However, both interactions shows same negative sign for the nearest-neighbor with distance of 1 unit cell. For my case, because of existence of minus sign of constant coupling $-J^2$, the negative susceptibility corresponds AFM interaction.

Figure 3.6(b) show the RKKY interactions of Ising spin 1-1 along x-direction and Ising spin 1-2 along y-direction. In its inset, both charge susceptibilities have a negative sign in short range distance or AFM.

$$J_{\alpha\beta}^{\mathrm{RKKY}}(\mathbf{R}) = \int_{-\pi}^{\pi}\int_{-\pi}^{\pi}\int_{-\pi}^{\pi}\int_{-\pi}^{\pi} \frac{dq_x dq_y dk_x dk_y}{(2\pi)^4} e^{-i\mathbf{q}\cdot\mathbf{R}} J_{\alpha\beta}(\mathbf{k},\mathbf{q}) \frac{n_F(E_{\mathbf{k}}) - n_F(E_{\mathbf{k}+\mathbf{q}})}{i\omega_n + E_{\mathbf{k}+\mathbf{q}} - E_{\mathbf{k}}} \tag{3.5}$$

$$(\text{where} \quad \mathbf{R} = \mathbf{R}_j - \mathbf{R}_i)$$

$$H^{\mathrm{RKKY}} \approx J_{\mathrm{NN}} \sum_{(\alpha\neq\beta)} \sigma_{i,\alpha}^z \sigma_{j,\beta}^z + J_{\mathrm{NNN}} \sum_{(\alpha=\beta)} \sigma_{i,\alpha}^z \sigma_{j,\beta}^z \quad (\text{With} \quad \alpha,\beta = 1,2), \tag{3.6}$$

$$(\text{ignore further neighbor interactions})$$

The model of Ising spin variables at the link of zero-flux square lattice, the nearest-neighbor interaction (J_{NN}) is Ising spin 1-2 pair, and the next-nearest-neighbor (J_{NNN}) coupling of Ising spin 1-1 and 2-2 pairs. Due to the results of real space and momentum space dependence of J^{RKKY}, the nearest-neighbor interaction ($J_{\mathrm{NN}} > 0$) and the next-nearest-neighbor ($J_{\mathrm{NNN}} > 0$) are AFM states. Our result for effective short-range interaction can be summarized in Eq. (3.6) with $\alpha, \beta = 1, 2$. The order vector $\mathbf{Q}_{\mathrm{o}} = (\pi, \pi)$ with formula $\mathbf{Q}_{\mathrm{o}} \cdot \mathbf{r}_m = 2\pi m$ (with m: label of unit cell) is used to determine the magnetic coupling [24]. The nearest same sign of spins is double of lattice vectors or distance of $2a$ (a is lattice constant). For the spin in the "site model" the nearest coupling is AFM, and the macroscopic magnetic order is an alternating AFM (Fig. 3.7(a)). So, the magnetic order of Ising spin in "link model" is $\mathbf{Q}_{\mathrm{o}} = (\pi, \pi)$,

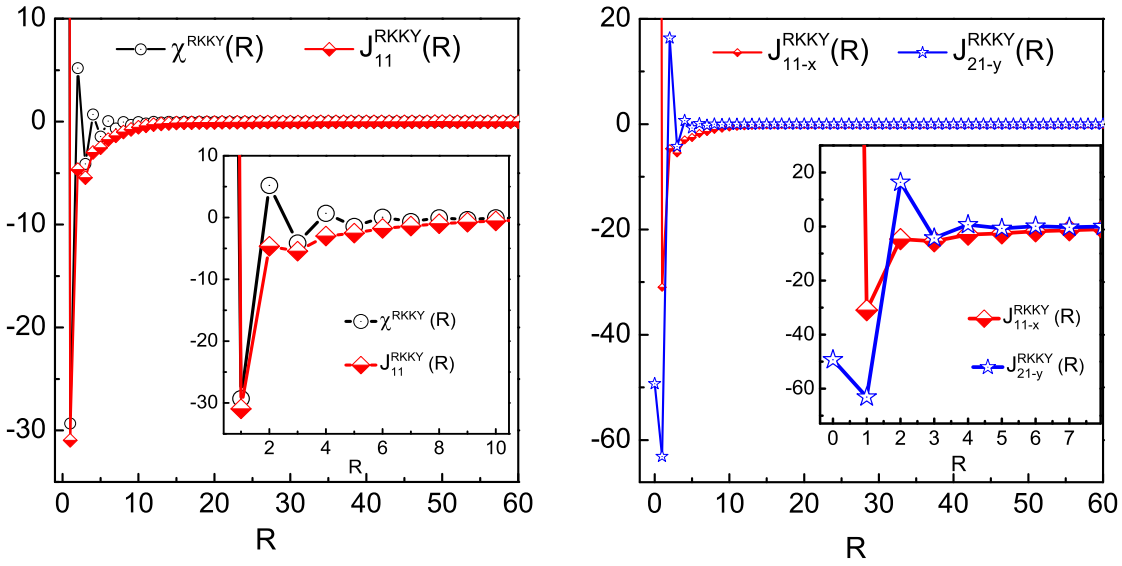

Figure 3.6. Real space dependence of (a) spin susceptibility $\chi^{\mathrm{RKKY}}(\mathbf{R})$ for "site model" and charge susceptibility $J_{11}^{\mathrm{RKKY}}(\mathbf{R})$ (Ising 1-1 interaction) along x-direction with lattice size $L = 120$ (because of the periodic boundary condition, we plot $\frac{L}{2} = 60$), and its inset rooms in short range of those interactions in 10 unit cells, (b) charge susceptibility for $J_{11}^{\mathrm{RKKY}}(\mathbf{R})$ (Ising spin 1-1 pair) and $J_{21}^{\mathrm{RKKY}}(\mathbf{R})$ (Ising spin 2-1 pair interaction) along x-direction, and its inset rooms in the short range interaction within 10 unit cells (where $R = |\mathbf{R}| = \frac{|\mathbf{R}_j - \mathbf{R}_i|}{a}$ is the distance of spins in two unit cell i and j, and $R = |j\hat{x} - i\hat{x}|$ and $R = |j\hat{y} - i\hat{y}|$ for x- and y-directions, respectively)

and macroscopic order seems to be similar. However, because of 2 spins in one unit cell, we have an alternative spin unit cells.

For our model, the existence of J_{NNN} and J_{NN} leads frustrating effect similar to the observation of spin-nematic model in real heavy fermion on $LiCuVO_4$ compounds [26]. This compound is a typical examples of frustrating effect in spin chain with the nearest-neighbor is FM coupling and next-nearest-neighbor is AFM coupling. Although both J_{NNN} and J_{NN} are AFM, there is existence of some FM couplings in nearest-neighbor pair (spin in diagonal stripe line). That is the reason why there is an appearance FM order of $Eigen1$ of charge suscpetibility $J_{2\times2}^{\mathrm{RKKY}}(\mathbf{q})$ (Fig. 3.7(b)). In similar Fermi surface, shifting the spin position from vertex to link, magnetic or-

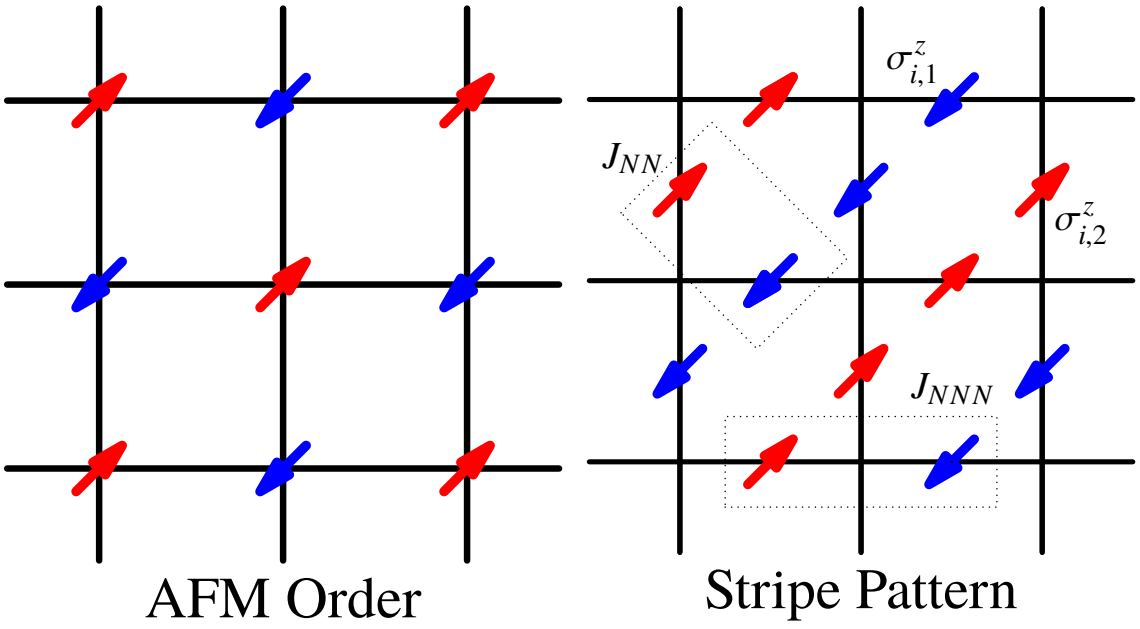

Figure 3.7. (a) Alternative (type-G) AFM pattern of "site model" (b) stripe AFM pattern of "link model" in zero-flux square lattice (red arrow and blue arrow represent spin up and spin down, respectively)

der changes from type-G AFM ("site model") to diagonal stripe AFM ("link model") (Fig. 3.7).

3.3 RKKY interaction in π-flux lattice

RKKY interaction for spin in "site model"

For the "site model" of π-flux lattice, there are two distinct atoms A and B (No Ising spins at the links in π-flux lattice Fig. 2.2) which correspond periodic spin lattice. That model is similar to magnetic impurity in graphene with effective Hamiltonian is written by matrix form:

$$\hat{H}_1 = \frac{-J^2}{N^2} \sum_{\mathbf{q}} \begin{pmatrix} \mathbf{S}_{\mathbf{q},\mathrm{A}} & \mathbf{S}_{\mathbf{q},\mathrm{B}} \end{pmatrix} J^{\mathrm{RKKY}}(\mathbf{q}, \omega_n) \begin{pmatrix} \mathbf{S}_{\mathbf{q},\mathrm{A}} \\ \mathbf{S}_{\mathbf{q},\mathrm{B}} \end{pmatrix}, \tag{3.7}$$

$$J^{\mathrm{RKKY}}(\mathbf{q},\omega_n)=\sum_{\mathbf{k}}\begin{bmatrix} J_{\mathrm{AA}}(\mathbf{k},\mathbf{q}) & J_{\mathrm{AB}}(\mathbf{k},\mathbf{q}) \\ J_{\mathrm{BA}}(\mathbf{k},\mathbf{q}) & J_{\mathrm{BB}}(\mathbf{k},\mathbf{q}) \end{bmatrix} \frac{n_F(E_{\mathbf{k},1})-n_F(E_{\mathbf{k}+\mathbf{q},2})}{i\omega_n+E_{\mathbf{k}+\mathbf{q},2}-E_{\mathbf{k},1}}. \tag{3.8}$$

All elements of 2×2 matrix of spin susceptibility $J^{\mathrm{RKKY}}(\mathbf{q})$ are listed below:

$$J_{\mathrm{AA}}(\mathbf{k},\mathbf{q})=\frac{\cos^2(k_y)\cos^2(k_y+q_y)}{\beta^2(\mathbf{k})\beta^2(\mathbf{k}+\mathbf{q})}, \tag{3.9}$$

$$J_{\mathrm{AB}}(\mathbf{k},\mathbf{q})=-\frac{(1+e^{i2k_y})[1+e^{i2(k_y+q_y}]\alpha(\mathbf{k})\alpha(\mathbf{k}+\mathbf{q})}{4\beta^2(\mathbf{k})\beta^2(\mathbf{k}+\mathbf{q})}, \tag{3.10}$$

$$J_{\mathrm{BA}}(\mathbf{k},\mathbf{q})=-\frac{(1+e^{-i2k_y})[1+e^{-i2(k_y+q_y}]\alpha(\mathbf{k})\alpha(\mathbf{k}+\mathbf{q})}{4\beta^2(\mathbf{k})\beta^2(\mathbf{k}+\mathbf{q})}, \tag{3.11}$$

$$J_{\mathrm{BB}}(\mathbf{k},\mathbf{q})=\frac{\alpha^2(\mathbf{k})\alpha^2(\mathbf{k}+\mathbf{q})}{\beta^2(\mathbf{k})\beta^2(\mathbf{k}+\mathbf{q})}. \tag{3.12}$$

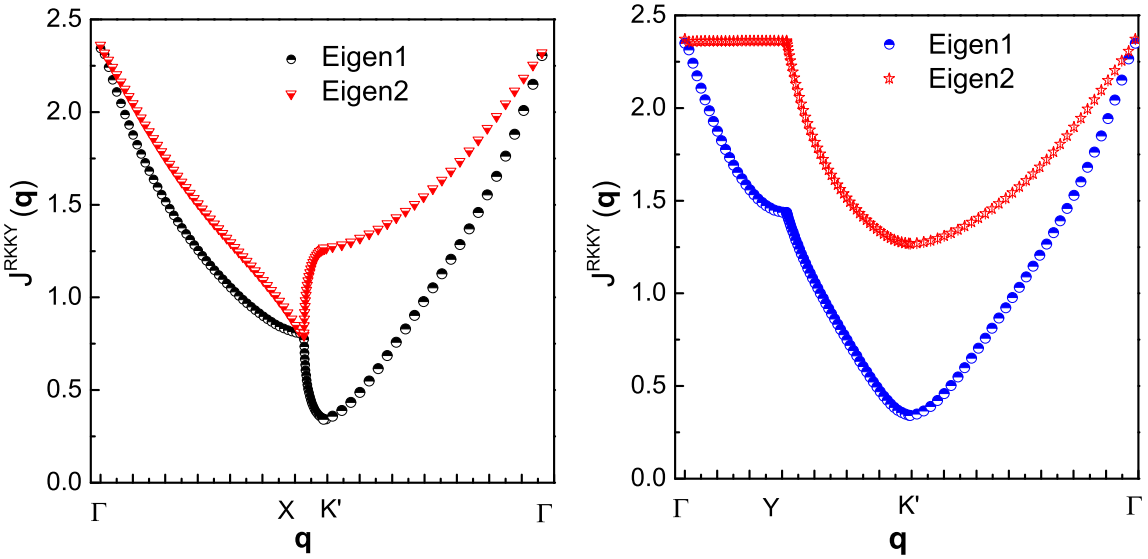

Figure 3.8. RKKY spin susceptibility versus momentum vector $J^{\mathrm{RKKY}}(\mathbf{q})$ with two eigenvalues *Eigen*1 and *Eigen*2 (lattice size $L=400$) along (a) Γ–X–K′–Γ and (b) Γ–Y–K′–Γ path of rectangular Brillouin zone ($\Gamma=(0,0)$, $\mathrm{X}=(\pi,0)$, and $\mathrm{K}'=(\pi,\frac{\pi}{2})$ and $\mathrm{Y}=(0,\frac{\pi}{2})$ in Fig. 3.1(b))

The non-interacting part $\hat{H}_0$ is similar to Ising model of π-flux lattice (two Dirac bands). The main part of spin susceptibility $J^{\mathrm{RKKY}}(\mathbf{q})$ for the π-flux is Linhard function (Eq. (3.8)). The interaction between impurity spins is driven by interband

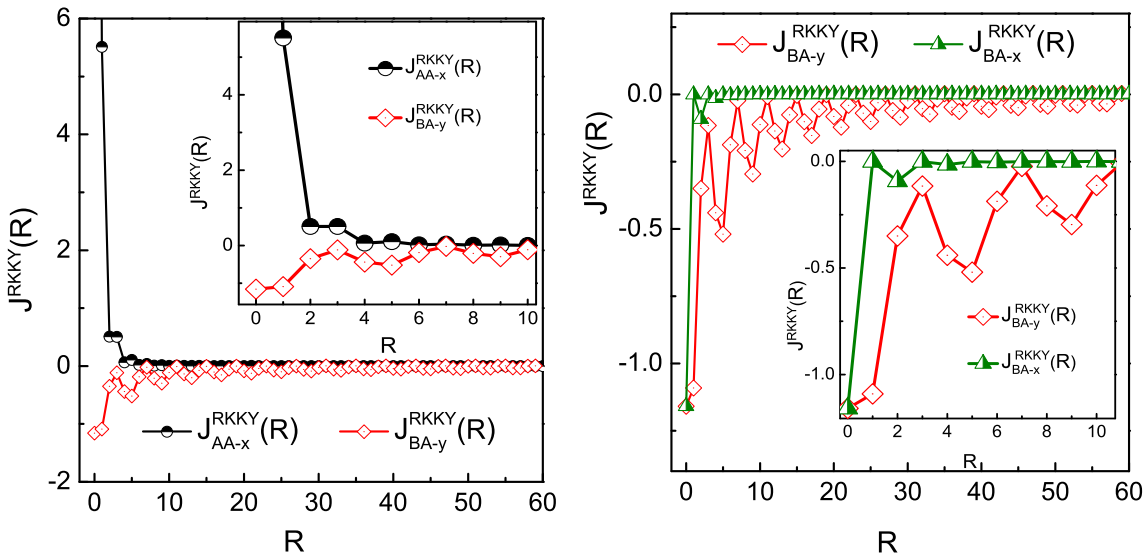

Figure 3.9. Real space RKKY spin susceptibility $J^{\mathrm{RKKY}}(\mathbf{R})$ (where $\mathbf{R} = \mathbf{R}_j - \mathbf{R}_i$ is the distance vector of two unit cells i and j) is calculated with lattice size $L = 120$ for (a) spins in same sublattice A–A and different sublattices B–A, (b) spins of different sublattices B–A in x- and y-directions (with distance of spin $R = |j\hat{x} - i\hat{x}|$, and $R = 2|j\hat{y} - i\hat{y}|$ for x- and y-directions, repsectively)

particle-hole symmetry (including hole or lower band, and electron or upper band) in contrast to intraband transition of zero-flux lattice. Because of no nesting wave vector, the ordering magnetic vector is determined at maximum or minimum points. For calculating of spin susceptibility $J^{\mathrm{RKKY}}(\mathbf{q})$, we take the integral the whole Brillouin zone with k_x from $-\pi$ to π and k_y from $-\frac{\pi}{2}$ to $\frac{\pi}{2}$. Because of the asymmetrical Brillouin zone in the π-flux lattice, that integration is taken two independent paths such as Γ–X–K$'$–Γ and Γ–X–K$'$–Γ paths (with $\Gamma = (0,0)$, X $= (\pi,0)$, and K$' = (\pi,\frac{\pi}{2})$ and Y $= (0,\frac{\pi}{2})$). 2×2 matrix structure of $J^{\mathrm{RKKY}}(\mathbf{q})$ is diagonalized to plot two different eigenvalues such as $Eigen1$ and $Eigen2$ (Fig. 3.8).

We observe two degenerate points such as Γ and X which correspond to maximum and minimum value of spin susceptibility $J^{\mathrm{RKKY}}(\mathbf{q})$. According to discussion of magnetic order above, the order vector is at the maximum or Γ point. So, ordering magnetic vector would be $\mathbf{Q}_{\mathrm{o}} = (0,0)$. I also calculate the eigenvector of 2×2

$J^{\mathrm{RKKY}}(\mathbf{q})$ matrix. At Γ point, $Eigen1$ gives V_1 eigenvector defines FM state, and V_2 of $Eigen2$ is AFM state (V_1 and V_2 eigenvectors are similar to "link model" of zero-flux lattice in Eq. (3.4)).

To construct the macroscopic magnetic pattern for "site model" of π-flux square lattice, the real space RKKY spin susceptibility $J^{\mathrm{RKKY}}(\mathbf{R})$ (where $\mathbf{R} = \mathbf{R}_j - \mathbf{R}_i$ is the distance vector of two unit cells i and j) is calculated (similar to "link model" of zero-flux lattice). Figure 3.9(a) shows that the real space of spin susceptibility $J^{\mathrm{RKKY}}_{\mathrm{AA}}(\mathbf{R})$ of same sublattice A–A (black half-filled circle) is positive magnitude and no sign-changing oscillation which correspond to FM coupling. The RKKY interaction of different sublattice $J^{\mathrm{RKKY}}_{\mathrm{AB}}(\mathbf{R})$ (red diamond)is the negative sign which is AFM state. Our results completely agree with the RKKY interaction of graphene [9, 10]. However, there is a different phenomena from graphene result is that the distance of spins in same sublattice and different sublattice is equal. That gives the effect of degenerate effect of eigenvalue spectrum in momentum space.

Figure 3.8(b) illustrates the interaction of spin in different sublattice B–A for two y- and x-direction which are armchair and zigzag ways, respectively. Inset of that figure shows that the zigzag interaction is suppressed faster than armchair one. The interaction of spins in zigzag direction is the next-nearest-neighbor coupling which is weaker that armchair, the nearest-neighbor pair. Therefore, we only consider the nearest-neighbor coupling in that model.

The macroscopic magnetic order of "site model" for π-flux lattice is drawn in figure 3.12(a) to give alternative line FM coupling of spins in same sublattice A–A and B–B. That result is similar to 2D type-A (or line-by-line) AFM order [33].

RKKY interaction for spin in "link model"

Similar work above, this section we calculate the momentum **a** dependence of charge susceptibility $\chi^{\mathrm{RKKY}}_{4\times4}(\mathbf{q},\omega_n)$ to find eigenvalues and corresponding eigenvectors (all terms of $M_{4\times4}(\mathbf{k},\mathbf{q})$ in Eq. (3.13) are shown in Eq. (2.38). Real space of charge susceptibility $\chi^{\mathrm{RKKY}}_{4\times4}(\mathbf{R}_{ij})$ (distance vector $\mathbf{R}_{ij}$ of two unit cells i and j) is computed using the discrete Fourier transformation.

$$\chi^{\mathrm{RKKY}}_{4\times4}(\mathbf{q},\omega_n)=\int_{-\pi}^{\pi}\int_{\frac{-\pi}{2}}^{\frac{\pi}{2}}\frac{dk_xdk_y}{4\pi^2}M_{4\times4}(\mathbf{k},\mathbf{q})\frac{n_F(E_{\mathbf{k},1})-n_F(E_{\mathbf{k}+\mathbf{q},2})}{i\omega_n+E_{\mathbf{k}+\mathbf{q},2}-E_{\mathbf{k},1}}. \tag{3.13}$$

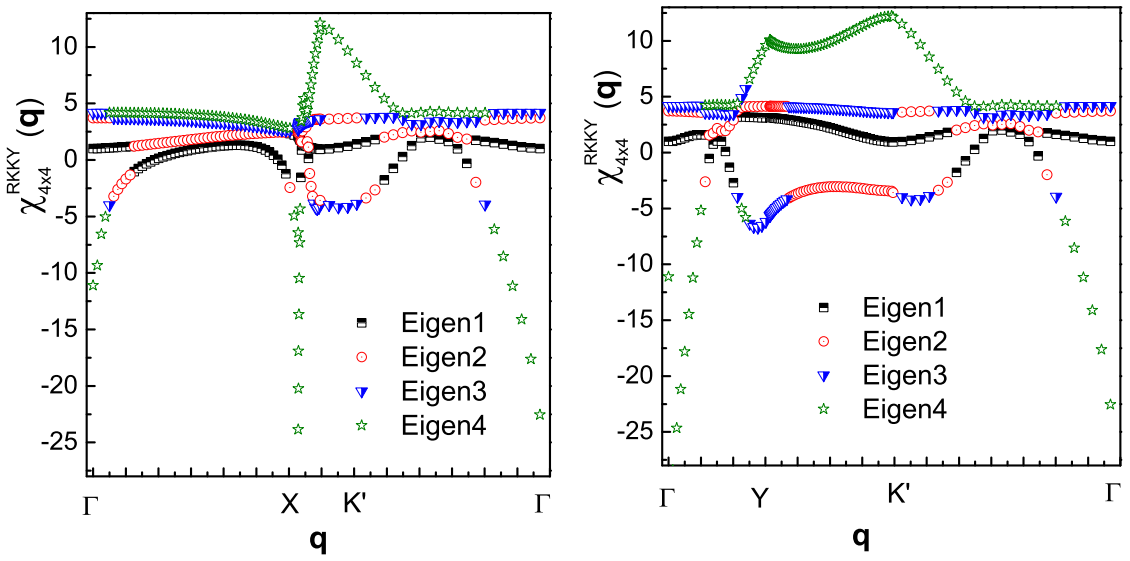

Figure 3.10. Eigenvalue plots of **q** space dependence of function $\chi^{\mathrm{RKKY}}_{4\times4}(\mathbf{q},\omega_n)$ along (a) Γ–X–K′–Γ and (b) Γ–Y–K′–Γ paths of rectangular Brillouin zone.

$$\chi^{\mathrm{RKKY}}_{\alpha\beta}(\mathbf{R})=\int_{-\pi}^{\pi}\int_{-\frac{\pi}{2}}^{\frac{\pi}{2}}\int_{-\pi}^{\pi}\int_{-\frac{\pi}{2}}^{\frac{\pi}{2}}\frac{dq_xdq_ydk_xdk_y}{(2\pi)^4}e^{-i\mathbf{q}\cdot\mathbf{R}}M_{\alpha\beta}(\mathbf{k},\mathbf{q})\frac{n_F(E_{\mathbf{k},1})-n_F(E_{\mathbf{k}+\mathbf{q},2})}{i\omega_n+E_{\mathbf{k}+\mathbf{q},2}-E_{\mathbf{k},1}} \tag{3.14}$$

$$(\text{where}\quad \mathbf{R}=\mathbf{R}_j-\mathbf{R}_i).$$

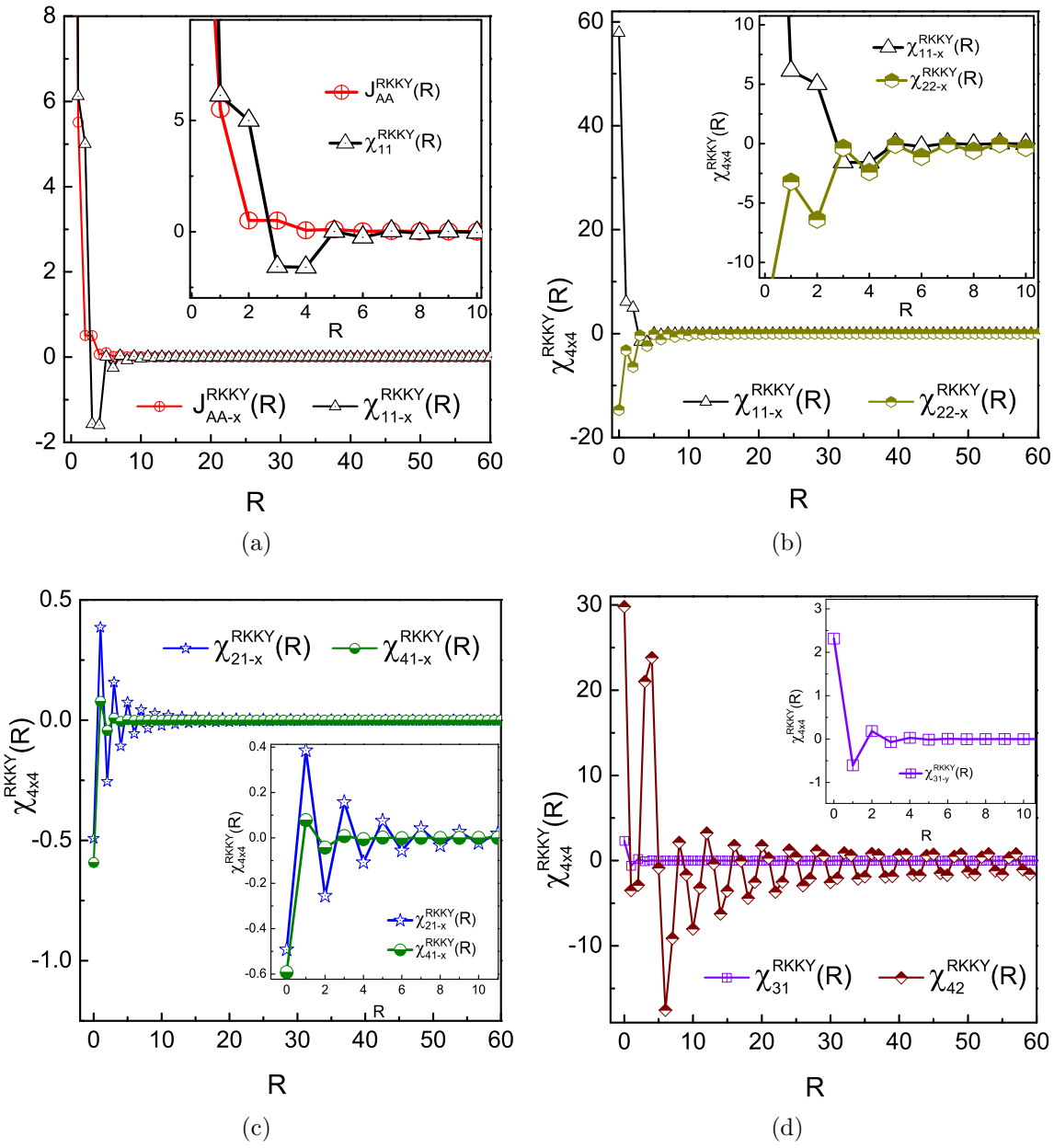

Figure 3.11. Real space RKKY interaction (a) charge susceptibility $\chi_{11}^{\mathrm{RKKY}}(\mathbf{R})$ of Ising spin 1-1 and spin susceptibility $J_{\mathrm{AA}}^{\mathrm{RKKY}}(\mathbf{R})$ of same sublattice spin A–A along x-direction with lattice size $L = 120$, (b) $\chi_{22}^{\mathrm{RKKY}}(\mathbf{R})$ of Ising spin 2-2 and $\chi_{11}^{\mathrm{RKKY}}(\mathbf{R})$ 1-1 along x-direction, (c) $\chi_{21-x}^{\mathrm{RKKY}}(\mathbf{R})$ of Ising spin 2-1 and $\chi_{41-x}^{\mathrm{RKKY}}(\mathbf{R})$ 4-1 in x-direction (like zigzag path in graphene), and (d) $\chi_{42-y}^{\mathrm{RKKY}}(\mathbf{R})$ of Ising spin 4-2, and $\chi_{31-x}^{\mathrm{RKKY}}(\mathbf{R})$ of Ising spin 3-1 along y-direction (similar to armchair path in graphene), (where $\mathbf{R} = \mathbf{R}_j - \mathbf{R}_i$ is the distance vector of two unit cells i and j, and $R = |\mathbf{R}| = |j\hat{x} - i\hat{x}|$, and $R = 2|j\hat{y} - i\hat{y}|$ for x- and y-directions, respectively).

First, Four different eigenvalues of 4×4 matrix of charge susceptibility are *Eigen*1, *Eigen*2, *Eigen*3, and *Eigen*4 (Fig. 3.10). They are plotted in two different

paths: Γ–X–K′–Γ and Γ–Y–K′–Γ paths. The maximum point of charge susceptibility is K′ = $(\pi, \pi/2)$ of the *Eigen*4 which defines the ordering magnetic vectors $\mathbf{Q}_{\rm o} = (\pi, \frac{\pi}{2})$.

Figure 3.11 illustrates the real space interactions of different Ising spins pair. Figure 3.11(a) shows the real space RKKY interactions of Ising spin 1-1 of "link model", and spin A–A of "site model" along x-direction. In contrast to no sign-change oscillation of spin susceptibility of spin A–A, the charge susceptibility of Ising spin 1-1 can reach negative value for 3 and 4 unit cells. So, the RKKY interaction is affected by momentum factor due to changing of spin position. Both of real functions concludes that the FM interaction for spin in nearest-neighbor pair (a distance of one unit cell).

In figure 3.11(b), the real space interaction of Ising spin 2-2 along x-direction is calculated. To compare with Ising spin 1-1, this interaction is complete AFM due to negative sign. The interactions of Ising spin 2-1 and 4-1 along x-direction is weak AFM because of small amplitude interaction (Fig. 3.11(c)). Those charge susceptibility are like zigzag interaction in graphene. The interaction of Ising 4-2 and 3-1 pairs along y-direction is so strong FM (Fig. 3.11(d)).

From momentum space RKKY interaction $\chi^{\rm RKKY}_{4\times4}(\mathbf{q})$, we define the ordering magnetic vector $\mathbf{Q}_{\rm o} = (\pi, \frac{\pi}{2})$ for "link model" of π-flux lattice. Beacuse π-flux model has four Ising spins in one unit cell, the mixing of FM and AFM couplings results in more complicated interaction than previous cases. The real space concludes that $\chi^{\rm RKKY}_{4\times4}(\mathbf{R})$ the interaction of next-nearest-neighbor ($J_{\rm NNN}$) (e.g Ising 1-1, 2-2 pair) is even stronger than the nearest-neighbor ($J_{\rm NN}$)interaction. That is typical properties of non-local RKKY interaction. Therefore, the high frustrating effect emerges strongly in that model. Based on above discussions, we draw magnetic order in terms of interaction pair to give the ferrimagnetic order which numbers of spin up is large than spin down ones. We also can consider this model as the FM clusters with the domain wall.

Figure 3.12 shows the magnetic order of "site model" and "link model" of in

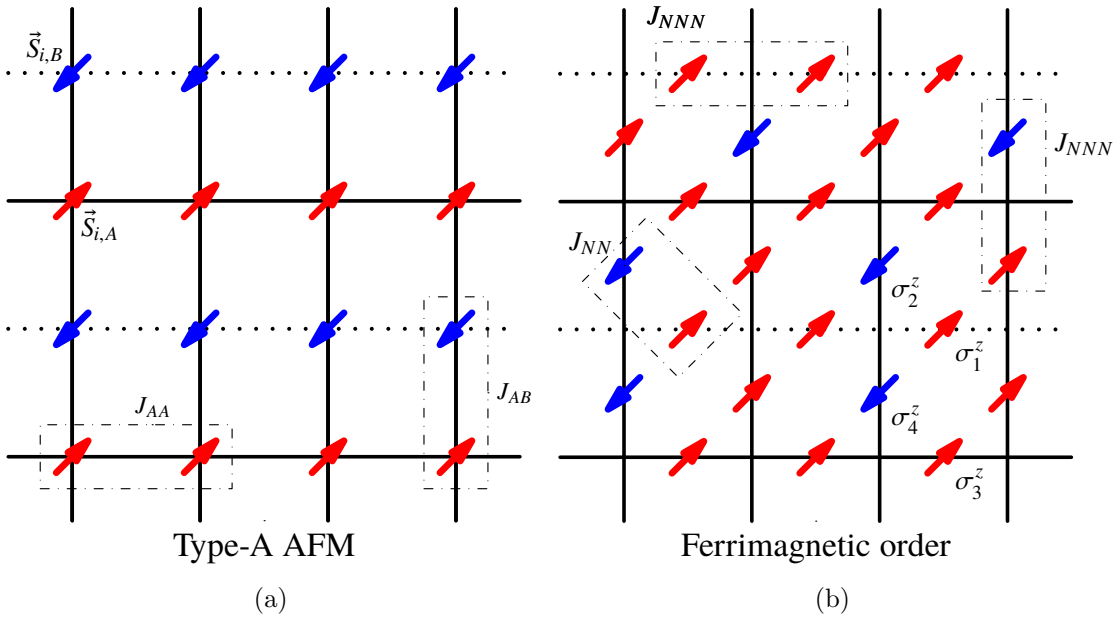

Figure 3.12. (a) AFM order of "site model" (b) ferrimagnetic order of "link model" in π-flux square lattice

π-flux square lattice. By changing the spin from site to link and double number of spin in one unit cell, the magnetic order is completely different such as type-A AFM for "site model" with wave vector $\mathbf{Q}_o = (0, 0)$ (Fig. 3.12(a)) and ferrimagnetic order of "link model" with wave vector $\mathbf{Q}_o = (\pi, \frac{\pi}{2})$ (Fig. 3.12(b)). Although our spin lattice is similar to X.Y. Xu's one [36], the magnetic coupling develops in different way because of considering of different magnetic interaction (RKKY for our model and transverse Ising spin of Xu's model). The competitive effect on next-nearest-neighbor and nearest-neighbor coupling lead the high frustrating effect in our model. That is a prototypical example of frustrated case or spin glass observed with RKKY interaction [18].

CHAPTER 4

CONCLUSIONS

We considered the model of Ising spins on the links of the square lattice, coupled to the fermions charge fluctuations for the zero-flux and π-flux cases. Unit cell of the π-flux lattice is doubled with respect to zero-flux one. The Brillouin zone changed from symmetrical square for zero-flux to asymmetrical rectangular of π-flux lattice. At the half-filling, the tight binding parts of Hamiltonian provide continuous metallic band and semimetallic Dirac band for zero- and π-flux models, respectively. We are observe the conventional Fermi surface with nesting wave vector, and Fermi points in Dirac bands for two cases.

RKKY interaction between Ising spins variables at the link is mediated by fermion in zero-flux and π-flux lattices. The second-order perturbation theory is used to calculate the charge susceptibility of Ising spins in "link model" to compare with conventional spin susceptibility of "site model". The increasing number of spins in a unit cell results in the matrix form of RKKY interaction with common factor of static Linhard function. In order to construct the magnetic order of each case, both real space and momentum space of RKKY interactions are considered.

First, for zero-flux square lattice, shifting spin from vertex ("site model") to the link ("link model"), the interacting distance of spins is changed a factor of $\frac{\sqrt{2}}{2}$ with the lattice constant a. The magnetic order vectors of two models are similar ($\mathbf{Q}_{\mathrm{o}} = (\pi, \pi)$ because of the strong nesting effect of Fermi surface which provides the singularity of static Linhard function. However, the interaction is clearly effective to magnetic order with its changing from type-G AFM to stripe AFM for "site model" and "link

model" respectively. Our result seem to be similar to the one by I. Tivinidze which the FM order is built with double lattice constant a of interacting length [34]. Due to long-range correlating property of RKKY interaction, competing and frustrating effects emerge in Ising spin model.

Second, for π-flux lattice, the RKKY interactions are in form of 2×2 and 4×4 matrices for "site model" and "link model", respectively. Because of no nesting properties in Fermi surface, the ordering vector is determined by obtaining the maximum value of eigenvalue of momentum RKKY interaction at the symmetric points. The spin susceptibility of "site model" is similar to the magnetic impurity in graphene. The interaction of same sublattice is FM whereas its different sublattice is AFM. There is difference from graphene model is the length of interaction in π-flux model is the interacting lengths are equal to give rise to degenerate phenomenon in the maximum point $\Gamma = (0, 0)$. For "link model", the magnetic interaction is most complicated situation which is competing of FM and AFM couplings in nearest-neighbor and next-nearest-neighbor pairs. That effect lead the high frustrating phenomena in "link model" of π-flux lattice. The magnetic order vectors are different in two cases such as $\mathbf{Q}_{\mathrm{o}} = (0, 0)$ and $(\pi, \frac{\pi}{2})$ for "site model" and "link model" respectively. Therefore, magnetic order changes from type-A AFM ("site model") to ferrimagnetic order ("link model").

Various magnetic orders in the ground state are observed in our models. That result is strongly supported by competing effect and many ground different states of 2D square models [6, 16, 36]. Our result can contribute to the rich variety of phenomena in 2D lattice. Particularly, the FM state is more interested in 2D experimental observation [18]. Moreover, for our models, we only consider a case of coupling J between spin and fermion in weak limit. Our future work will continue with strong coupling case (like the Kondo effect [11]), inserting the interacting Hubbard term [7, 27], and tuning the filling factor [16].

BIBLIOGRAPHY

BIBLIOGRAPHY

[1] ad E. J. Lee, C. L. K. (2005), Z_2 topological order and quantum spin Hall effect, *Physical Review Letter*, 95, 146,802.

[2] Affleck, I., and J. B. Marston (1988), Large-n limit of the Heisenberg-Hubbard model: Implication for high-T_c superconductors, *Physical Review B*, 37, 3774–3777.

[3] Allerdt, A., C. A. Büsser, G. B. Martins, and A. E. Geiguin (2015), Kondo versus indirect exchange: Role of lattice and actual range of RKKY interactions in real materials, *Physical Review B*, 91, 085,101.

[4] Altland, A., and B. Simons (2010), *Condensed Matter Field Theory*, 2 ed., Cambrige University Press.

[5] Ashcroft, N. W., and N. D. Mermin (1975), *Solid State Physics*, 3 ed., Thomson Learning, Cornell University.

[6] Assaad, F. F., and T. Grover (2016), Simple fermionic model of deconfined phases and phase transitions, *Physical Review X*, 6, 041,049.

[7] Assaad, F. F., M. Bercx, and M. Hohenadler (2013), Topological invariant and quantum spin models from magnetic π fluxes in correlated topological insulators, *Physical Review X*, 3, 011,015.

[8] Beach, K. S. (2004), Magnetic-field-induced antiferromagnetism in Kondo lattice, Ph.D. thesis, Massachusetts Institute of Technology.

[9] Black-Schaffer, A. M. (2010), RKKY coupling graphene, *Physical Review B*, 81, 205,416.

[10] Brey, L., H. A. Fertig, and S. D. Sarma (2007), Dilute graphene antiferromagnet, *Physical Review Letter*, 99, 116,802.

[11] Coleman, P. (2015), *Introduction to Many-Body Physics*, Cambridge University Press.

[12] Coleman, P., and A. H. Nevidomskyy (2010), Frustration and the Kondo effect in heavy fermion materials, *Journal of Low Temperature Physics*, 161, 182.

[13] Doniach, S. (1977), Kondo lattics and weak antiferromagnetism, *Physica B + C*, 91B.

[14] Fischer, B., and M. W. Klein (1975), Magnetic and nonmagnetic impurities in two-dimensional metals, *Physical Review B*, 11, 2025.

[15] Flint, R., and T. Senthil (2013), Chiral RKKY interaction in $Pr_2Ir_2O_7$, *Physical Review B*, 87, 125,147.

[16] Gazit, S., M. Randeria, and A. Vishwanath (2017), Emergent Dirac fermions and broken symmetries in confined and deconfined phases of Z_2 gauge theories, *Nature Physics*, 13, 041,049.

[17] Harris, A. B., T. C. Lubensky, and E. J. Mele (1989), Flux phases in two-dimensional tight-binding models, *Physical Review B*, 40, 2631–3634.

[18] Huang, B. (2017), Layer-dependent ferromagnetism in a Van der Waals crystal down to the monolayer limit, *Nature Letter*, 546, 270.

[19] Kauya, T. (1956), A theory of metallic ferro- and antiferromagnetism on Zener's model, *Progress of Theoretical Physics*, 16, 45.

[20] Kondo, J. (1962), G-shift and anomalous Hall effect in gadolium metals, *Progress of Theoretical Physics*, 28, 846.

[21] Kondo, J. (1964), Resistance minimum in dilute magnetic alloys, *Progress of Theoretical Physics*, 32, 37.

[22] Kotov, V. N., B. Uchoa, V. M. Pereira, F. Guinea, and A. H. C. Neto (2012), Electron-electron interactions in graphene: current status and perspectives, *Review of Modern Physics*, 84, 1067.

[23] Lee, S. B., A. Panamekanti, and Y. B. Kim (2013), RKKY interactions and the anomalous Hall effect in metallic rare-earth pyrochlores, *Physical Review Letter*, 111, 196,601.

[24] Legg, H. F., and B. Braunecker (2016), Spin liquid mediated RKKY interaction, *ArXiv*, arXiv:1612.06868.

[25] Neto, A. H. C., F. Guinea, N. M. R. Peres, K. S. Novoselov, and A. K. Geim (2008), Electron properties of graphene, *Review of Modern Physics*, 81, 109.

[26] Orlova, A. (2017), Nuclear magnetic resonance signature of the spin-nematic phase in $LiCuVO_4$ at high magntic fields, *Physical Review Letter*, 118, 247,201.

[27] Otsuka, Y., S. Yunoki, and S. Sorella (2016), Universal quantum criticality in the metal-insulator transition of two-dimensional interacting dirac electrons, *Physical Review X*, 6, 011,029.

[28] Roth, L. M., H. J. Zeiger, and T. A. Kaplan (1966), Geralization of the Ruderman-Kittel-Kasuya-Yosida interaction for nonspherical Fermi surfaces, *Physical Review*, 149, 519.

[29] Ruderman, M. A., and C. Kittel (1954), Indirect exchange coupling of nuclear magnetic moments by conduction electrons, *Physical Review*, 96, 99.

[30] Sakurai, J. J., and J. Napolitano (2010), *Modern Quatum Mechanics*, 2 ed., Pearson.

[31] Saremi, S. (2007), RKKY in half-filled bipartite lattices: graphene as an example, *Physical Review B*, 76, 184,430.

[32] She, J.-H., and A. R. Bishop (2013), RKKY interaction and intrinsic frustration in non-Fermi-liquid metals, *Physical Review Letter*, 111, 017,001.

[33] Sólyom, J. (2010), *Fundamentals of the Physics of Solids*, vol. 3, Springer, Budapest, Hungary.

[34] Tivinidze, I., A. Schwabe, and M. Potthoff (2014), Ferromagnetism of magnetic impurities coupled indirectly via conduction electrons: insights various theoretical approaches, *Physical Review B*, 90, 045,112.

[35] Uchoa, B., T. G. Rappoport, and A. H. C. Neto (2011), Kondo quantum criticality of magnetic adatoms in graphene, *Physical Review Letter*, 106, 016,801.

[36] Yan, X. X., B. K. S. D., F. F. Assaad, and Z. Y. Meng (2017), Topological phase transitions with SO(4) symmetry in (2+1)D interacting Dirac fermions, *Phys. Rev. B*, 95, 085,110.

APPENDICES

APPENDIX A

A.1 Theorems and Indentities

A.1.1 Wick's theorem for fermions

N-point correlation function with fermion operator:

$$\langle \phi_{j_1}\phi_{j_2}...\phi_{j_n}\bar{\phi_{i_n}}...\bar{\phi_{i_2}}\bar{\phi_{i_1}}\rangle = \sum_P (\mathrm{sgn}(P)) A^{-1}_{j_1 i_{P_1}}...A^{-1}_{j_n i_{P_n}} \tag{A.1}$$

Here, each term is $\langle \phi_j \bar{\phi_i}\rangle = A^{-1}_{ji}$ and P is the number of permutation [4].

A.1.2 Matsubara frequency summation

The Matsubara frequencies for fermion is : $\omega_n = (2n+1)\pi T$ (n is the integer and T is the temperature) [4].

A.2 RKKY interaction of zero-flux model

A.2.1 Overlap term

$$\langle \Psi_2|\Psi_1\rangle = \frac{J^2}{N^2}\sum_{\mathbf{k},\mathbf{q}}\sum_{\mathbf{k}',\mathbf{q}'}(A\sigma^z_{\mathbf{q},1}+B\sigma^z_{\mathbf{q},2})(A'\sigma^z_{\mathbf{q}',1}+B'\sigma^z_{\mathbf{q}',2})\,\langle\Psi_{gs}|\, c^\dagger_{\mathbf{k}}(t)c^\dagger_{\mathbf{k}+\mathbf{q}}(t)c^\dagger_{\mathbf{k}'}c_{\mathbf{k}'+\mathbf{q}'}\,|\Psi_{gs}\rangle \tag{A.2}$$

With A, B, A', and B' are defined as:

$$A = e^{-i\mathbf{k}\cdot\mathbf{a_1}} + e^{i(\mathbf{k}+\mathbf{q})\cdot\mathbf{a_1}} \qquad B = e^{i\mathbf{k}\cdot\mathbf{a_2}} + e^{-i(\mathbf{k}+\mathbf{q})\cdot\mathbf{a_2}}$$

$$A' = e^{-i\mathbf{k}'\cdot\mathbf{a_1}} + e^{i(\mathbf{k}'+\mathbf{q}')\cdot\mathbf{a_1}} \qquad B' = e^{-i\mathbf{k}'\cdot\mathbf{a_2}} + e^{i(\mathbf{k}'+\mathbf{q}')\cdot\mathbf{a_2}}$$

So the effective interacting Hamiltonian $\hat{H}_1$ is:

$$\hat{H}_1 = \frac{J^2}{N^2}\sum_{\mathbf{k},\mathbf{q}}\sum_{\mathbf{k}',\mathbf{q}'}(A\sigma^z_{\mathbf{q},1} + B\sigma^z_{\mathbf{q},2})(A'\sigma^z_{\mathbf{q}',1} + B'\sigma^z_{\mathbf{q}',2}) \left\langle\Psi_{gs}\right| \left[\hat{n}(\mathbf{k},\mathbf{q},t), \hat{n}(\mathbf{k}',\mathbf{q}',t)\right] \left|\Psi_{gs}\right\rangle \tag{A.3}$$

with $\hat{n}(\mathbf{k},\mathbf{q},t) = c^\dagger_{\mathbf{k}}(t)c_{\mathbf{k}+\mathbf{q}}(t)$: density operator of electron.

A.2.2 Derivation of equation of motion

Non-interacting Hamitonian $\hat{H}_0$:

$$\hat{H}_0 = \sum_{\mathbf{k}\sigma} E_{\mathbf{k}\sigma}c^\dagger_{\mathbf{k}\sigma}c_{\mathbf{k}\sigma} \tag{A.4}$$

Time dependence annihilation operator is following:

$$c_{\mathbf{k}\sigma}(t) = e^{i\hat{H}_0 t}c_{\mathbf{k}\sigma}e^{-i\hat{H}_0 t} \tag{A.5}$$

Using the anticomutation relation of fermion second quantization operators.

And the order time-dependence differential equation of that operator is derived follow-

ing:

$$\begin{aligned}\frac{dc_{\mathbf{k}\sigma}(t)}{dt} &= iE_{\mathbf{k}\sigma}e^{i\hat{H}_0 t}[\hat{H}_0, c_{\mathbf{k}\sigma}]e^{-i\hat{H}_0 t} \\ &= -iE_{\mathbf{k}\sigma}e^{i\hat{H}_0 t}c_{\mathbf{k}\sigma}e^{-i\hat{H}_0 t} \\ &= -iE_{\mathbf{k}\sigma}c_{\mathbf{k}\sigma}(t)\end{aligned} \tag{A.6}$$

The first order differentialequation is solved to give the formulas of creation and annihilation operators:

$$c_{\mathbf{k}\sigma}(t) = e^{iE_{\mathbf{k}\sigma}t}c_{\mathbf{k}\sigma} \tag{A.7}$$

$$c^{\dagger}_{\mathbf{k}\sigma}(t) = e^{iE_{\mathbf{k}\sigma}t}c^{\dagger}_{\mathbf{k}\sigma} \tag{A.8}$$

A.2.3 Derivation of Linhard function

Detail Linhard function is showed in reference [33]. The Linhard function can be derived in many ways such as using Green's function and second quatization. This part, I show the derivation of dynamics Linhard function using second quatization methods. It is started from overlap term of equation A.2 to form 4-point correlation function:

$$\sum_{\mathbf{k}\mathbf{k}'} \langle \Psi_{gs}|\, c^{\dagger}_{\mathbf{k}}(t)c_{\mathbf{k}+\mathbf{q}}(t)c^{\dagger}_{\mathbf{k}'}c_{\mathbf{k}'+\mathbf{q}'}\, |\Psi_{gs}\rangle \tag{A.9}$$

This sum describes the propagation of an electron-hole pair from time 0 when electron is annihilated to time t when hole is created. The electron-hole pair can be created only if the state with wave vector $\mathbf{k}$ is occupied in ground state, while the state with $\mathbf{k}+\mathbf{q}$ is empty as a excited state. Using Wick's theorem and equation of motion methods to decouple the correlation function.

$$\sum_{\mathbf{k}\mathbf{k}'} \langle \Psi_{gs}| \, c^{\dagger}_{\mathbf{k}}(t) c_{\mathbf{k}+\mathbf{q}}(t) c^{\dagger}_{\mathbf{k}'} c_{\mathbf{k}'+\mathbf{q}'} \, |\Psi_{gs}\rangle \quad = \sum_{\mathbf{k}} e^{iE_{\mathbf{k}}t} e^{-iE_{\mathbf{k}+\mathbf{q}}t} \langle \Psi_{gs}| \, c^{\dagger}_{\mathbf{k}} c_{\mathbf{k}} \, |\Psi_{gs}\rangle$$
$$(1 - \langle \Psi_{gs}| \, c^{\dagger}_{\mathbf{k}+\mathbf{q}} c_{\mathbf{k}+\mathbf{q}} \, |\Psi_{gs}\rangle)$$
$$= \sum_{\mathbf{k}} e^{iE_{\mathbf{k}}t} e^{-iE_{\mathbf{k}+\mathbf{q}}t} n_F(E_{\mathbf{k}})[1 - n_F(E_{\mathbf{k}+\mathbf{q}})]$$

With $n_F(E_{\mathbf{k}}) = \langle \Psi_{gs}| \, c^{\dagger}_{\mathbf{k}} c_{\mathbf{k}} \, |\Psi_{gs}\rangle$ is called the Fermi distribution function. We transform that correlation function in real time t to Matsubara frequency ω_n. This correlation is analytic in the upper complex half-plane, and insert a factor $\exp(-\delta|t|)$ with infinitesimal element δ, which is equivalent to switching on the perturbation adiabatically. The Fourier transformation is then:

$$\begin{aligned} \int_{-\infty}^{\infty} \theta(t) e^{i\omega t} e^{i(E_{\mathbf{k}} - E_{\mathbf{k}+\mathbf{q}})} e^{-\delta|t|} dt &= \int_{0}^{\infty} e^{i(\omega + E_{\mathbf{k}} - E_{\mathbf{k}+\mathbf{q}} + i\delta)t} dt \\ &= \frac{i}{\omega + i\delta + E_{\mathbf{k}} - E_{\mathbf{k}+\mathbf{q}}} \\ &= \frac{i}{i\omega_n + E_{\mathbf{k}} - E_{\mathbf{k}+\mathbf{q}}} \end{aligned} \tag{A.10}$$

Finally, that overlap term gives us:

$$f(\mathbf{q}, \omega_n) = \sum_{\mathbf{k}} n_F(E_{\mathbf{k}})[1 - n_F(E_{\mathbf{k}+\mathbf{q}})] \frac{i}{i\omega_n + E_{\mathbf{k}} - E_{\mathbf{k}+\mathbf{q}}} \tag{A.11}$$

Analogously, the second term of the commutator:

$$\sum_{\mathbf{k}\mathbf{k}'} \langle \Psi_{gs}| \, c^{\dagger}_{\mathbf{k}'} c_{\mathbf{k}'+\mathbf{q}'} c^{\dagger}_{\mathbf{k}}(t) c_{\mathbf{k}+\mathbf{q}}(t) \, |\Psi_{gs}\rangle \tag{A.12}$$

Take step-by-step similarly above, that gives us:

$$g(\mathbf{q},\omega_n) = \sum_{\mathbf{k}} n_F(E_{\mathbf{k+q}})[1 - n_F(E_{\mathbf{k}})]\frac{i}{i\omega_n + E_{\mathbf{k}} - E_{\mathbf{k+q}}} \tag{A.13}$$

So, the Linhard function is defined by taking the imaginary part of $Im(f(\mathbf{q},\omega_n) - g(\mathbf{q},\omega_n))$ with $\omega_n = (2n+1)T$ is the Matsubara frequency (Defined on appendix A).

$$\chi(\mathbf{q},\omega_n) = -\sum_{\mathbf{k}} \frac{n_F(E_{\mathbf{k}}) - n_F(E_{\mathbf{k+q}})}{i\omega_n + E_{\mathbf{k+q}} - E_{\mathbf{k}}} \tag{A.14}$$

Finally the first term of equation A.3 gives the effective interaction between Ising spins 1-1, 1-2, 2-1, and 2-2 in $\mathbf{q}$ space:

$$\begin{aligned} M_{11}(\mathbf{q}) &= \sigma^z_{\mathbf{q},1}\sigma^z_{-\mathbf{q},1}\sum_{\mathbf{k}}[e^{-ik_x} + e^{i(k_x+q_x)}][e^{ik_x} + e^{-i(k_x+q_x)}]\chi(\mathbf{k},\mathbf{q},\omega_n) \\ &= \sigma^z_{\mathbf{q},1}\sigma^z_{-\mathbf{q},1}\sum_{\mathbf{k}}[2 + e^{i(2k_x+q_x)} + e^{-i(2k_x+q_x)}]\chi(\mathbf{k},\mathbf{q},\omega_n) \end{aligned} \tag{A.15}$$

$$M_{12}(\mathbf{q}) = \sigma^z_{\mathbf{q},1}\sigma^z_{-\mathbf{q},2}\sum_{\mathbf{k}}[e^{-i(k_x+k_y+q_y)}+e^{i(k_x+k_y+q_x)}+e^{-i(k_x-k_y)}+e^{i(k_x-k_y+q_x-k_y)}]\chi(\mathbf{k},\mathbf{q},\omega_n) \tag{A.16}$$

$$M_{21}(\mathbf{q}) = \sigma^z_{\mathbf{q},2}\sigma^z_{-\mathbf{q},1}\sum_{\mathbf{k}}[e^{i(k_x+k_y+q_y)}+e^{-i(k_x+k_y+q_x)}+e^{i(k_x-k_y)}+e^{-i(k_x-k_y+q_x-k_y)}]\chi(\mathbf{k},\mathbf{q},\omega_n) \tag{A.17}$$

$$
\begin{aligned}
M_{22}(\mathbf{q}) &= \sigma^z_{\mathbf{q},2}\sigma^z_{-\mathbf{q},2}\sum_{\mathbf{k}}[e^{-ik_y}+e^{i(k_y+q_y)}][e^{ik_y}+e^{-i(k_y+q_y)}]\chi(\mathbf{k},\mathbf{q},\omega_n) \\
&= \sigma^z_{\mathbf{q},2}\sigma^z_{-\mathbf{q},2}\sum_{\mathbf{k}}[2+e^{i(2k_y+q_y)}+e^{-i(2k_y+q_y)}]\chi(\mathbf{k},\mathbf{q},\omega_n)
\end{aligned}
\tag{A.18}
$$

A.3 RKKY Interaction of π-flux model

A.3.1 Unitary tranformation

$$
\begin{aligned}
\hat{H}_0 &= \begin{bmatrix} c^\dagger_{\mathbf{k}A} & c^\dagger_{\mathbf{k}B} \end{bmatrix} H_{\mathbf{k}} \begin{bmatrix} c_{\mathbf{k}A} \\ c_{\mathbf{k}A} \end{bmatrix} \\
&= \begin{bmatrix} c^\dagger_{\mathbf{k}A} & c^\dagger_{\mathbf{k}B} \end{bmatrix} U_{2\times2} E_{\mathbf{k}} U^*_{2\times2} \begin{bmatrix} c_{\mathbf{k}A} \\ c_{\mathbf{k}A} \end{bmatrix}
\end{aligned}
\tag{A.19}
$$

where $U_{2\times2}$ and $E_{\mathbf{k}}$ are 2×2 matrices of unitary transformation between the fermion and quasiparticle basis, and diagonalized energy, repectively. $U^*_{2\times2}$ is the Hermitian conjugate of of unitary matrix $U_{2\times2}$. The explicit unitary transformation between two basis is shown below:

$$
\begin{aligned}
c^\dagger_{\mathbf{k}A} &= \sum_{n=1,2} f^\dagger_{\mathbf{k}n} U^*_{n,A,\mathbf{k}} & \qquad c^\dagger_{\mathbf{k}B} &= \sum_{n=1,2} f^\dagger_{\mathbf{k}n} U^*_{n,B,\mathbf{k}} \\
c_{\mathbf{k}A} &= \sum_{n=1,2} U_{n,A,\mathbf{k}} f_{\mathbf{k}n} & \qquad c_{\mathbf{k}B} &= \sum_{n=1,2} U_{n,B,\mathbf{k}} f_{\mathbf{k}n}
\end{aligned}
$$

A.3.2 Interacting Hamiltonian

The interacting Hamiltonian in momentum space is:

$$\hat{H}_1 = -\frac{J}{N}\sum_{\mathbf{k},\mathbf{q}}\Big\{\sigma^z_{\mathbf{q},1}c^\dagger_{\mathbf{k},B}c_{\mathbf{k}+\mathbf{q},B}(e^{-ik_x}+e^{i(k_x+q_x)}) + \sigma^z_{\mathbf{q},2}[e^{-i2k_y}c^\dagger_{\mathbf{k},A}c_{\mathbf{k}+\mathbf{q},B} + e^{i2(k_y+q_y)} c^\dagger_{\mathbf{k},B}c_{\mathbf{k}+\mathbf{q},A}] - \sigma^z_{\mathbf{q},3}c^\dagger_{\mathbf{k},A}c_{\mathbf{k}+\mathbf{q},A}(e^{-ik_x}+e^{i(k_x+q_x)}) + \sigma^z_{\mathbf{q},4}[c^\dagger_{\mathbf{k},A}c_{\mathbf{k}+\mathbf{q},B} + c^\dagger_{\mathbf{k},B}c_{\mathbf{k}+\mathbf{q},A}]\Big\}$$

Similar to calculating the effective interacting Hamiltonian $\hat{H}_1$ of zero-flux lattice, we have total sixteen term of interaction in π-flux model. The ground state of π-flux model at half-filling or chemical potential $\mu = 0$ is:

$$|\Psi_{gs}\rangle = \prod_{\mathbf{k}<\mathbf{k}_F} f^\dagger_{\mathbf{k}\tau,1}|0\rangle \quad (\mathbf{k}_F : \text{Fermi momentum}) \tag{A.20}$$

The first term of the effective interaction is:

$$\begin{aligned} I_{11}(\mathbf{q},\mathbf{q}') &= \sum_{\mathbf{k},\mathbf{k}'}\left[e^{-ik_x}+e^{i(k_x+q_x)}\right]\left[e^{-ik'_x}+e^{i(k'_x+q'_x)}\right]\sigma^z_{\mathbf{q},1}\sigma^z_{\mathbf{q}',1}\langle\Psi_{gs}|\left[c^\dagger_{\mathbf{k},B}(t)c^\dagger_{\mathbf{k}+\mathbf{q},B}(t), c^\dagger_{\mathbf{k}',B}c_{\mathbf{k}'+\mathbf{q}',B}\right]|\Psi_{gs}\rangle \\ &= \sum_{\mathbf{k},\mathbf{k}'}\sum_{n_2,n'_2,N_2,N'_2}\left[e^{-ik_x}+e^{i(k_x+q_x)}\right]\left[e^{-ik'_x}+e^{i(k'_x+q'_x)}\right]\sigma^z_{\mathbf{q},1}\sigma^z_{\mathbf{q}',1}U^*_{\mathbf{k},n_2,B}U_{\mathbf{k}+\mathbf{q},n'_2,B}U^*_{\mathbf{k}',N_2,B}U_{\mathbf{k}'+\mathbf{q}',N'_2,B} \\ &\qquad \langle\Psi_{gs}|\left[f^\dagger_{\mathbf{k},n_2}(t)f_{\mathbf{k}+\mathbf{q},n'_2}(t), f^\dagger_{\mathbf{k}',N_2}f_{\mathbf{k}'+\mathbf{q}',N'_2}\right]|\Psi_{gs}\rangle \end{aligned} \tag{A.21}$$

So, we will get ($\mathbf{k} = \mathbf{k}' + \mathbf{q}'$ and $\mathbf{k}' = \mathbf{k} + \mathbf{q}$):

$$I_{11}(\mathbf{q}) = \sigma^z_{\mathbf{q},1}\sigma_{\mathbf{q}',1}\sum_{\mathbf{k}}\left[2+e^{i(2k_x+q_x)}+e^{-i(2k_x+q_x)}\right]\frac{\alpha^2(\mathbf{k})\alpha^2(\mathbf{k}+\mathbf{q})}{\beta^2(\mathbf{k})\beta^2(\mathbf{k}+\mathbf{q}}\chi(\mathbf{k},\mathbf{q},\omega_n) \tag{A.22}$$

Other interacting terms are derived similarly. Final structure of interaction Hamilto-

nian $\hat{H}_1$ is the 4×4 matrix.

$$
\begin{aligned}
M_{11}(\mathbf{k},\mathbf{q}) &= 4\cos^2\big(k_x+\frac{q_x}{2}\big)\frac{\alpha^2(\mathbf{k})\alpha^2(\mathbf{k}+\mathbf{q})}{\beta^2(\mathbf{k})\beta^2(\mathbf{k}+\mathbf{q}}, \\
M_{12}(\mathbf{k},\mathbf{q}) &= \big\{\alpha(\mathbf{k})[-e^{-i2(k_y+q_y)}-e^{-i4(k_y+q_y)}]+\alpha(\mathbf{k}+\mathbf{q})(1+e^{i2k_y})\big\}(e^{-ik_x}+e^{i(k_x+q_x)}) \\
&\quad \frac{\alpha(\mathbf{k})\alpha(\mathbf{k}+\mathbf{q})}{2\beta^2(\mathbf{k})\beta^2(\mathbf{k}+\mathbf{q})}, \\
M_{13}(\mathbf{k},\mathbf{q}) &= \frac{\cos^2(k_x+\frac{q_x}{2})\alpha(\mathbf{k})\alpha(\mathbf{k}+\mathbf{q})[1+e^{-i2(k_y+q_y)}][1+e^{-i2k_y}]}{\beta^2(\mathbf{k})\beta^2(\mathbf{k}+\mathbf{q})}, \\
M_{14}(\mathbf{k},\mathbf{q}) &= \{\alpha(\mathbf{k})[-1-e^{-i2(k_y+q_y)}]+\alpha(\mathbf{k}+\mathbf{q})(1+e^{-i2k_y})\}(e^{-ik_x}+e^{i(k_x+q_x)}) \\
&\quad \frac{\alpha(\mathbf{k})\alpha(\mathbf{k}+\mathbf{q})}{2\beta^2(\mathbf{k})\beta^2(\mathbf{k}+\mathbf{q})}, \\
M_{21}(\mathbf{k},\mathbf{q}) &= \{\alpha(\mathbf{k})[-e^{i2(k_y+q_y)}-e^{i4(k_y+q_y)}]+\alpha(\mathbf{k}+\mathbf{q})(1+e^{-i2k_y})\}(e^{ik_x}+e^{-i(k_x+q_x)}) \\
&\quad \frac{\alpha(\mathbf{k})\alpha(\mathbf{k}+\mathbf{q})}{2\beta^2(\mathbf{k})\beta^2(\mathbf{k}+\mathbf{q})}, \\
M_{22}(\mathbf{k},\mathbf{q}) &= \frac{1}{4\beta^2(\mathbf{k})\beta^2(\mathbf{k}+\mathbf{q})}\{e^{-i(4k_y+2q_y)}(1+e^{i2k_y})(-1-e^{-i2(k_y+q_y)})\alpha(\mathbf{k})\alpha(\mathbf{k}+\mathbf{q}) \\
&\quad +(2+e^{i2k_y}+e^{-i2k_y})\alpha^2(\mathbf{k}+\mathbf{q})+[2+e^{i2(k_y+q_y)}+e^{-i2(k_y+q_y)}]\alpha^2(\mathbf{k}) \\
&\quad -e^{i(4k_y+2q_y)}(1+e^{-i2k_y})[1+e^{i2(k_y+q_y)}]\alpha(\mathbf{k})\alpha(\mathbf{k}+\mathbf{q})\}, \\
M_{23}(\mathbf{k},\mathbf{q}) &= \frac{[e^{-i(k_x+q_x)}+e^{ik_x}][1+e^{-i2k_y}][1+e^{-i2(k_y+q_y)}]}{8\beta^2(\mathbf{k})\beta^2(\mathbf{k}+\mathbf{q})}\{\alpha(\mathbf{k}+\mathbf{q})(1+e^{i2k_y}) \\
&\quad +\alpha(\mathbf{k})[-1-e^{i2(k_y+q_y)}]\}, \\
M_{24}(\mathbf{k},\mathbf{q}) &= \frac{1}{4\beta^2(\mathbf{k})\beta^2(\mathbf{k}+\mathbf{q})}\{e^{-i2k_y}(1+e^{i2k_y})(-1-e^{-i2(k_y+q_y)})\alpha(\mathbf{k})\alpha(\mathbf{k}+\mathbf{q}) \\
&\quad +e^{-i2k_y}(2+e^{i2k_y}+e^{-i2k_y})\alpha^2(\mathbf{k}+\mathbf{q})+e^{i2(k_y+q_y)}[2+e^{i2(k_y+q_y)} \\
&\quad +e^{-i2(k_y+q_y)}]\alpha^2(\mathbf{k})-e^{i2(k_y+q_y)}(1+e^{-i2k_y})[1+e^{i2(k_y+q_y)}]\alpha(\mathbf{k})\alpha(\mathbf{k}+\mathbf{q})\},
\end{aligned}
$$

$$
\begin{aligned}
M_{31}(\mathbf{k},\mathbf{q}) &= \frac{\cos^2(k_x+\frac{q_x}{2})\alpha(\mathbf{k})\alpha(\mathbf{k}+\mathbf{q})[1+e^{i2(k_y+q_y)}][1+e^{i2k_y}]}{\beta^2(\mathbf{k})\beta^2(\mathbf{k}+\mathbf{q})},\\
M_{32}(\mathbf{k},\mathbf{q}) &= \frac{[e^{i(k_x+q_x)}+e^{-ik_x}][1+e^{i2k_y}][1+e^{i2(k_y+q_y)}]}{8\beta^2(\mathbf{k})\beta^2(\mathbf{k}+\mathbf{q})}\{\alpha(\mathbf{k}+\mathbf{q})(1+e^{-i2k_y})\\
&\quad +\alpha(\mathbf{k})[-1-e^{-i2(k_y+q_y)}]\},\\
M_{33}(\mathbf{k},\mathbf{q}) &= 4\cos^2(k_x+\frac{q_x}{2})\frac{\cos^2(k_y)\cos^2(k_y+q_y)}{\beta^2(\mathbf{k})\beta^2(\mathbf{k}+\mathbf{q})},\\
M_{34}(\mathbf{k},\mathbf{q}) &= \frac{[e^{-i(k_x+q_x)}+e^{ik_x}][1+e^{i2k_y}][1+e^{i2(k_y+q_y)}]}{8\beta^2(\mathbf{k})\beta^2(\mathbf{k}+\mathbf{q})}\{\alpha(\mathbf{k})(-1-e^{-i2(k_y+q_y)})\\
&\quad +\alpha(\mathbf{k}+\mathbf{q})(1+e^{-i2k_y})\},\\
M_{41}(\mathbf{k},\mathbf{q}) &= \{\alpha(\mathbf{k})[-1-e^{i2(k_y+q_y)}]+\alpha(\mathbf{k}+\mathbf{q})(1+e^{i2k_y})\}(e^{ik_x}+e^{-i(k_x+q_x)})\\
&\quad \frac{\alpha(\mathbf{k})\alpha(\mathbf{k}+\mathbf{q})}{2\beta^2(\mathbf{k})\beta^2(\mathbf{k}+\mathbf{q})},\\
M_{42}(\mathbf{k},\mathbf{q}) &= \frac{1}{4\beta^2(\mathbf{k})\beta^2(\mathbf{k}+\mathbf{q})}\{e^{i2k_y}(1+e^{-i2k_y})(-1-e^{i2(k_y+q_y)})\alpha(\mathbf{k})\alpha(\mathbf{k}+\mathbf{q})\\
&\quad +e^{i2k_y}(2+e^{i2k_y}+e^{-i2k_y})\alpha^2(\mathbf{k}+\mathbf{q})+e^{-i2(k_y+q_y)}[2+e^{i2(k_y+q_y)}\\
&\quad +e^{-i2(k_y+q_y)}]\alpha^2(\mathbf{k})-e^{-i2(k_y+q_y)}(1+e^{i2k_y})[1+e^{-i2(k_y+q_y)}]\alpha(\mathbf{k})\alpha(\mathbf{k}+\mathbf{q})\},\\
M_{43}(\mathbf{k},\mathbf{q}) &= \frac{[e^{-i(k_x+q_x)}+e^{ik_x}][1+e^{-i2k_y}][1+e^{-i2(k_y+q_y)}]}{8\beta^2(\mathbf{k})\beta^2(\mathbf{k}+\mathbf{q})}\{\alpha(\mathbf{k})(-1-e^{i2(k_y+q_y)})\\
&\quad +\alpha(\mathbf{k}+\mathbf{q})(1+e^{i2k_y})\},\\
M_{44}(\mathbf{k},\mathbf{q}) &= \frac{1}{4\beta^2(\mathbf{k})\beta^2(\mathbf{k}+\mathbf{q})}\{(1+e^{i2k_y})(-1-e^{-i2(k_y+q_y)})\alpha(\mathbf{k})\alpha(\mathbf{k}+\mathbf{q})\\
&\quad +(2+e^{i2k_y}+e^{-i2k_y})\alpha^2(\mathbf{k}+\mathbf{q})+[2+e^{i2(k_y+q_y)}+e^{-i2(k_y+q_y)}]\alpha^2(\mathbf{k})\\
&\quad -(1+e^{-i2k_y})[1+e^{i2(k_y+q_y)}]\alpha(\mathbf{k})\alpha(\mathbf{k}+\mathbf{q})\}.
\end{aligned}
$$

VITA

HUU TRAN DO

No. 10 · Stewart Street · Oxford Mississippi · email: htdo@go.olemiss.edu

EDUCATION:

B. S, Materials Science and Engineering, Hanoi University of Science and Technology, August 2013

TEACHING EXPERIENCE:

Teaching Assistant, 2016-2017

University of Mississippi

Physics 221, 222.